J. Fluid Mech. (2006), *vol.* 562, *pp.* 83–121.
doi:10.1017/S0022112006000929 Printed in the United Kingdom

Wave turbulence in rapidly rotating flows

By F. BELLET, F. S. GODEFERD, J. F. SCOTT AND C. CAMBON†

Laboratoire de Mécanique des Fluides et d'Acoustique UMR 5509, École Centrale de Lyon, France

(Received 14 October 2004 and in revised form 27 January 2006)

An asymptotic quasi-normal Markovian (AQNM) model is developed in the limit of small Rossby number Ro and high Reynolds number, i.e. for rapidly rotating turbulent flow. Based on the 'slow' amplitudes of inertial waves, the kinetic equations are close to those that would be derived from Eulerian wave-turbulence theory. However, for their derivation we start from an EDQNM statistical closure model in which the velocity field is expanded in terms of the eigenmodes of the linear wave regime. Unlike most wave-turbulence studies, our model accounts for the detailed anisotropy as the angular dependence in Fourier space. Nonlinear equations at small Rossby number are derived for the set e, Z, h – energy, polarization anisotropy, helicity – of spectral quantities which characterize second-order two-point statistics in anisotropic turbulence, and which generate every quadratic moment of inertial wave amplitudes. In the simplest symmetry consistent with the background equations, i.e. axisymmetry without mirror symmetry, e, Z and h depend on both the wavevector modulus k and its orientation θ to the rotation axis. We put the emphasis on obtaining accurate numerical simulations of a generalized Lin equation for the angular-dependent energy spectrum $e(k, \theta, t)$, in which the energy transfer reduces to integrals over surfaces given by the triadic resonant conditions of inertial waves. Starting from a pure three-dimensional isotropic state in which e depends only on k and $Z = h = 0$, the spectrum develops an inertial range in the usual fashion as well as angular anisotropy. After the development phase, we observe the following features:

(*a*) A k^{-3} power law for the spherically averaged energy spectrum. However, this is the average of power laws whose exponents vary with the direction of the wavevector from k^{-2} for wavevectors near the plane perpendicular to the rotation axis, to k^{-4} for parallel wavevectors.

(*b*) The spectral evolution is self-similar. This excludes the possibility of a purely two-dimensional large-time limit.

(*c*) The energy density is very large near the perpendicular wavevector plane, but this singularity is integrable. As a result, the total energy has contributions from all directions and is not dominated by this singular contribution.

(*d*) The kinetic energy decays as $t^{-0.8}$, an exponent which is about half that one without rotation.

1. Introduction

Rotation of the reference frame is an important factor in some mechanisms of flow instability, and the study of rotating flows is interesting from the point of view

† Author to whom correspondence should be addressed: claude.cambon@ec-lyon.fr

of turbulence modelling in fields as diverse as engineering (e.g. turbomachinery and reciprocating engines with swirl and tumble), geophysics and astrophysics. Effects of mean curvature or of advection by a large eddy can be tackled using similar approaches.

Even where excluding altogether mean velocity and temperature gradients in the rotating frame of reference, the role of the Coriolis forces is still subtle and difficult to model, since the corresponding linear dynamics is made up of oscillating motions, from the presence of neutral dispersive waves. In contrast with shear flows, there is no direct production of energy by linear effects, and the alteration of the distribution of energy is mainly controlled by nonlinear interactions, such as resonantly interacting waves for instance. Given the complexity of this general problem, we restrict our study to the case of homogeneous turbulence, assuming unbounded flows.

From several experimental, theoretical and numerical studies, in which rotation is suddenly applied to decaying homogeneous turbulence, some generally accepted statements are summarized as follows (Bardina, Ferziger & Rogallo 1985; Cambon & Jacquin 1989; Jacquin *et al.* 1990; Cambon, Jacquin & Lubrano 1992; Cambon, Mansour & Godeferd 1997, referred to herein as CMG).†

(i) Rotation inhibits the energy cascade, so that the dissipation rate is reduced.

(ii) The initial three-dimensional isotropy is broken through nonlinear interactions modified by rotation, so that anisotropy develops. This anisotropy may be characterized for instance by the angular distribution of energy in spectral space.

(iii) If turbulence is initially anisotropic, the 'rapid' effects of rotation are short-time-scale linear dynamics which may be tackled as in rapid distortion theory. They conserve the directional anisotropy and damp polarization anisotropy, resulting in a spectacular change of their relative contributions to the Reynolds stress tensor anisotropy.

Although the energy density associated with the plane of wavevectors perpendicular to the rotation axis can become very large due to the angular transfer, this does not necessarily mean that the flow approaches a two-dimensional state, in the sense that the overall energy is dominated by wavevectors near the plane. A careful application of the Taylor–Proudman theorem only shows that the 'slow manifold' is the two-dimensional manifold at small Rossby number. But it does not imply the transition from three-dimensional to two-dimensional turbulence, which is a nonlinear transfer mechanism of energy from all the modes towards the two-dimensional ones; in other words from 'rapid' to 'slow' ones. Two-dimensionalization can be predicted using the Proudman theorem under two conditions: small nonlinearity and slow motion. The first condition is fulfilled at small Rossby number but not necessarily the second. In physical space, the slow, two-dimensional, manifold is the vertically averaged velocity field, such that $\partial/\partial z = 0$, whereas in Fourier space it is the wave plane normal to the rotation axis. Results illustrating the mathematical subtleties arising from rapid rotation and dependence on the type of initial conditions can be found in Babin, Mahalov & Nicolaenko (1997, 1999, 2001).

Two-point statistical closure (TPC) models have been extensively exploited to predict the nonlinear interactions, with satisfactory quantitative comparisons with direct numerical simulations (DNS) (CMG; Godeferd & Cambon 1994; Godeferd & Staquet 2003). The mathematical formalism used in these previous studies has shown that it is fruitful to expand the fluctuating velocity field using the eigenmodes of

† Other recent DNS and LES studies are discussed in § 7.

the linear operator associated with the waves, as well as for analysing the nonlinear interactions in terms thereof. Similar eigenmodes decompositions (helical modes) were used by Cambon & Jacquin (1989), Waleffe (1993), Smith & Waleffe (1999) and Morinishi, Nakabayshi & Ren (2001*a*). Anisotropic eddy-damped quasi-normal Markovian (EDQNM), models in terms of helical modes will therefore be discussed to some extent in § 2.

Regarding wave-turbulence (WT) theory which has been studied for a long time (see e.g. Benney & Saffman 1966), recent mathematical developments have renewed interest in flows which consist of superimposed dispersive waves, in which nonlinear interactions drive the long-time behaviour (Caillol & Zeitlin 2000; Lvov & Tabak 2001; Galtier 2003; Galtier *et al.* 2000). The link between the velocity $\boldsymbol{u}$ of a wave, given its wavevector $\boldsymbol{k}$, and its amplitude $\boldsymbol{a}$ can be established as

$$\boldsymbol{u}(\boldsymbol{x}, t) = \boldsymbol{a}(t) \exp[\mathrm{i}(\boldsymbol{k} \cdot \boldsymbol{x} - \sigma t)] \tag{1.1}$$

provided the analytical dispersion law $\sigma = \pm\sigma_k$ is known (Greenspan 1968). The nonlinear equations obtained from WT and TPC for the averaged amplitudes appear to be very similar, as briefly discussed next.

The statistical homogeneity and quasi-normal assumptions used in TPC have counterparts in WT, obtained by assuming *a priori* random phases for the wave field.† The corresponding isotropic version of the quasi-normal assumption is discussed in Staquet & Sommeria (2002). Moreover, *isotropic* dispersion laws such that $\sigma_k = |\boldsymbol{k}|^\alpha$ in (1.1) are almost exclusively treated in WT for deriving Kolmogorov spectra, with the key hypothesis of constant isotropic energy fluxes across different scales associated with a wavenumber $|\boldsymbol{k}|$ (Zakharov, Lvov & Falkovich 1992). This contrasts with geophysical flows, in which dispersion laws are anisotropic: $\sigma_k = \beta k_x / k^2$ in the case of Rossby waves, and $\sigma_k = 2\Omega k_\parallel / k$ for inertial waves $\sigma_k = N k_\perp / k$ for internal gravity waves; k_x, $k_\parallel$ and $k_\perp$ are the wavevector components respectively in the zonal direction and the directions parallel and perpendicular to the rotation/gravity axes. In the latter two three-dimensional cases, anisotropy manifests itself in the conical shape of iso-phase surfaces in experiments with localized forcing. Vertical plane cuts of these surfaces yield a 'St-Andrew cross' pattern, as observed in the experiments by McEwan (1970), Mowbray & Rarity (1967), and numerically reproduced by Godeferd & Lollini (1999). Nonlinear interactions between waves also reflect anisotropy in the angular-dependent energy drain.

When considering Eulerian correlations, TPC and WT theories share a wide common background, seldom commented on in the literature. Both WT and homogeneous TPC provide equations for the slow evolution of the wave mean spectral energy densities. The energy transfer terms are cubic in terms of the wave amplitude, from triadic interactions. In WT only are fourth-order transfer terms considered, from quartet interactions, when triple resonance is explicitly prevented by the dispersion law itself, or by geometrical constraints. This occurs for instance in shallow-water waves. When triple resonances exist, as in rotating, stably stratified and MHD turbulence (Caillol & Zeitlin 2000; Galtier *et al.* 2000), WT kinetic equations have the same structure as their counterpart in anisotropic TPC. Hence, WT and TPC have a common limit at very small interaction parameter, e.g. Rossby number Ro, Froude number Fr, and magnetic Reynolds number in MHD. We shall show

† The random phase approximation is commonly used by physicists. On the other hand, a mathematical justification for the quasi-normal relationship can be established in the weakly nonlinear limit of wave turbulence, following Benney & Newell (1969).

that the precise form of the eddy damping parameter, which remains the heuristic correction to quasi-normal transfer in EDQNM, is unimportant in this limit. Its only role is to regularize the resonance operators. Beyond the weak nonlinearity assumption, the eddy damping, or more generally the nonlinear contribution to Kraichnan's response function (Kraichnan 1958), can regain some importance for moderate interaction parameters, in allowing extrapolation from WT through TPC towards a larger domain, until the case of strong interactions is reached (e.g. pure isotropic turbulence without external or wave effects, for which classic multi-point closure models work satisfactorily).

The paper is organized as follows. A survey of previous EDQNM models based on the helical mode decomposition is given in § 2, with their link to a rapid–slow analysis. Kinetic equations in the asymptotic limit of small Rossby number are derived for e, Z, h in § 3. The numerical method is presented in § 4, numerical results are given in § 5, with recapitulation, discussion and perspectives in § 6. A conclusion is proposed in § 7. Tensorial details and tedious algebra are reported in Appendices A to D. Appendix E provides details of the numerical procedure.

2. EDQNM in terms of the eigenmodes of inertial wave motion

2.1. *The helical mode decomposition*

Rotating turbulence can be related to studies of incompressible homogeneous turbulence in the presence of a mean flow with space-uniform velocity gradients (Craya 1958; Cambon & Scott 1999), provided a pure antisymmetric form $\epsilon_{ikj}\Omega_k$ is chosen, with $\boldsymbol{\Omega}$ the angular velocity. It is nevertheless simpler to work with a coordinate system and velocity vectors in the rotating frame. In this non-inertial frame, rotation induces inertial centrifugal and Coriolis forces. Since the former can be incorporated in the pressure term, only the latter has to be taken into account in the Navier–Stokes equations in the rotating frame,

$$(\partial_t + \boldsymbol{u}\cdot\nabla)\,\boldsymbol{u} + 2\Omega\boldsymbol{n}\times\boldsymbol{u} + \nabla p - \nu\nabla^2\boldsymbol{u} = 0, \tag{2.1}$$

$$\nabla\cdot\boldsymbol{u} = 0, \tag{2.2}$$

for the fluctuating velocity $\boldsymbol{u}$ and the pressure p divided by density. The unit vector $\boldsymbol{n}$ denotes the direction aligned with the angular velocity of the rotating frame $\boldsymbol{\Omega} = \Omega\boldsymbol{n}$. Without loss of generality the fixed frame of reference is chosen such that $n_i = \delta_{i3}$. Therefore u_3 is the axial velocity component.

In the inviscid linear regime, equation (2.1) becomes

$$\frac{\partial\boldsymbol{u}}{\partial t} + 2\Omega\times\boldsymbol{u} + \nabla p = 0. \tag{2.3}$$

Since the Coriolis force is not divergence-free, the pressure term makes a non-trivial contribution to maintain the incompressibility constraint (2.2). The velocity can be eliminated between the latter equation and the Poisson equation for the pressure, for which a closed form is found:

$$\partial_t^2(\nabla^2 p) + 4\Omega^2\nabla_\parallel^2 p = 0. \tag{2.4}$$

The reduced Laplacian operator along the axis of rotation is $\nabla_\parallel^2$. Although the primitive Poisson equation $\nabla^2 p = f$ is parabolic, equation (2.4) is hyperbolic and admits propagating waves solutions. Interesting properties of these inertial waves are illustrated by cross-shaped visualizations in the experiment by McEwan (1970).

Seeking plane-wave solutions of (2.4) such that $p \propto \mathrm{e}^{\mathrm{i}(\boldsymbol{k}\cdot\boldsymbol{x}-\sigma t)}$, one finds the dispersion law of inertial waves

$$\sigma = \pm\sigma_k, \quad \sigma_k = 2\Omega\frac{k_\parallel}{k} = 2\Omega\cos\theta, \tag{2.5}$$

where θ is the angle between $\boldsymbol{k}$ and the rotation vector $\boldsymbol{\Omega}$. Without pressure, only the horizontal part of the flow is affected by circular periodic motion at constant frequency 2Ω, but propagating waves cannot occur. Hence the fluctuating pressure is responsible both for anisotropic dispersivity and for horizontal–vertical coupling, coming from the divergence-free condition.

An equation similar to (2.4) is found for the vertical velocity component, and more generally for both the poloidal and toroidal potentials, detailed in Appendix A. Without local forcing and boundary conditions, the linear problem can be nicely recast in Fourier space as

$$\frac{\partial\hat{u}_i}{\partial t} + 2\Omega P_{in}\epsilon_{n3j}\hat{u}_j = 0 \tag{2.6}$$

for the velocity Fourier coefficient $\hat{\boldsymbol{u}}(\boldsymbol{k},t)$. The projection tensor is $P_{in} = \delta_{in} - k_i k_n/k^2$, δ_{in} is the Kronecker tensor, and ϵ_{ijk} the alternating tensor. In the turbulence community, (2.6) is known as the rapid distortion theory equation (RDT, as a reminder of the rapid–slow time scale separation implied when linearizing).

Given the incompressibility constraint $\hat{\boldsymbol{u}}\cdot\boldsymbol{k} = 0$, it is easier to project the equation in the plane orthogonal to $\boldsymbol{k}$, using the frame $(\boldsymbol{e}^{(1)}, \boldsymbol{e}^{(2)})$ (see the definition (A 3) of these vectors in Appendix A). The linear solution consists of a rotation of the initial Fourier component $\hat{\boldsymbol{u}}(\boldsymbol{k},0)$ about the $\boldsymbol{k}$-axis by an angle $(2\Omega k_\parallel/k)t = \sigma_k t$. A tractable diagonal form of the corresponding Green's function is found in terms of the two complex eigenvectors $\boldsymbol{N} = \boldsymbol{e}^{(2)} - \mathrm{i}\boldsymbol{e}^{(1)}$ and $\boldsymbol{N}^* = \boldsymbol{N}(-\boldsymbol{k}) = \boldsymbol{e}^{(2)} + \mathrm{i}\boldsymbol{e}^{(1)}$ in the plane normal to $\boldsymbol{k}$, namely

$$G_{ij}^{RDT}(\boldsymbol{k},t,t') = \frac{1}{2}\sum_{s=\pm1} N_i(s\boldsymbol{k})N_j(-s\boldsymbol{k})\mathrm{e}^{\mathrm{i}s\sigma_k(t-t')} \tag{2.7}$$

which generates the linear solutions

$$\hat{u}_i(\boldsymbol{k},t) = G_{ij}^{RDT}(\boldsymbol{k},t,t')\hat{u}_j(\boldsymbol{k},t').$$

These vectors have been used by different authors for two decades (Cambon & Jacquin 1989), and are called here helical modes after Waleffe (1993). $\boldsymbol{N}$ and $\boldsymbol{N}^*$ prove useful in the pure rotation context since they provide a diagonal decomposition, for they are the eigenmodes of the curl operator, and therefore form a complete basis on which to project the Navier–Stokes equations. The resulting equations appear to be more tractable for discussing both linear and nonlinear operators, as well as for designing closure theories for turbulence, be it with rotation or not. Upon defining the velocity amplitudes ξ_1, ξ_{-1} along $\boldsymbol{N}$ and $\boldsymbol{N}^*$ such that

$$\hat{\boldsymbol{u}}(\boldsymbol{k},t) = \xi_+(\boldsymbol{k},t)\boldsymbol{N}(\boldsymbol{k}) + \xi_-(\boldsymbol{k},t)\boldsymbol{N}(-\boldsymbol{k}), \tag{2.8}$$

the linear inviscid solution is

$$\xi_s(\boldsymbol{k},t) = \xi_s(\boldsymbol{k},0)\exp\left(2\mathrm{i}s\Omega t\frac{k_\parallel}{k}\right), \quad s = \pm1. \tag{2.9}$$

In terms of these modes, the complete nonlinear equation becomes

$$\left(\frac{\partial}{\partial t}+\nu k^2-\mathrm{i}s\left(2\Omega\frac{k_\parallel}{k}\right)\right)\xi_s=\sum_{s',s''=\pm1}\int_{\boldsymbol{k}+\boldsymbol{p}+\boldsymbol{q}=\boldsymbol{0}} m_{ss's''}(\boldsymbol{k},\boldsymbol{p})\xi^*_{s'}(\boldsymbol{p},t)\xi^*_{s''}(\boldsymbol{q},t)\,\mathrm{d}^3\boldsymbol{p}, \quad (2.10)$$

in which the left-hand side linear operator is diagonal, and the right-hand side is the modified form of the quadratic nonlinear term, exhibiting the interaction operator $\boldsymbol{m}$. In this way, one may separate the rapid oscillating part of the complete nonlinear solution of (2.10) from slowly varying amplitudes a_s, $s=\pm1$, as in multiple-time-scale analysis. The solution is formally written as

$$\xi_s(\boldsymbol{k},t)=a_s(\boldsymbol{k},t)\exp\left(2\mathrm{i}s\Omega t\frac{k_\parallel}{k}\right), \quad s=\pm1, \quad (2.11)$$

and from (2.8) the ith component of the Fourier coefficient of the velocity is

$$\hat{u}_i(\boldsymbol{k},t)=\sum_{s=\pm1}a_s(\boldsymbol{k},t)\exp(\mathrm{i}s\sigma_k t)N_i(s\boldsymbol{k}). \quad (2.12)$$

In the evolution equation for the slow amplitudes a_s, the linear operators are absorbed into the nonlinear one, as integrating factors:

$$\dot{a}_s+\nu k^2 a_s=\sum_{s',s''=\pm1}\int_{\boldsymbol{k}+\boldsymbol{p}+\boldsymbol{q}=\boldsymbol{0}}\exp\left(-2\mathrm{i}\Omega\left(s\frac{k_\parallel}{k}+s'\frac{p_\parallel}{p}+s''\frac{q_\parallel}{q}\right)t\right)$$
$$\times m_{ss's''}(\boldsymbol{k},\boldsymbol{p})a^*_{s'}(\boldsymbol{p},t)a^*_{s''}(\boldsymbol{q},t)\,\mathrm{d}^3\boldsymbol{p} \quad (2.13)$$

with the influence matrix $m_{ss's''}$ given in Cambon & Jacquin (1989), Waleffe (1993). Equation (2.13) demonstrates the importance of the resonant triads $\sigma_k\pm\sigma_p\pm\sigma_q=0$ that appear when the phase term in (2.13) is zero:

$$\frac{k_\parallel}{k}\pm\frac{p_\parallel}{p}\pm\frac{q_\parallel}{q}=0 \quad \text{with} \quad \boldsymbol{k}+\boldsymbol{p}+\boldsymbol{q}=0. \quad (2.14)$$

Resonant and almost resonant triads are expected to dominate nonlinear slow motion, since significant non-zero values of $k_\parallel/k\pm p_\parallel/p\pm q_\parallel/q$ on the right-hand side of (2.13) severely damp the nonlinearity by scrambling. In that case, why not obtain a simplified model by solving equation (2.13) with an integral restricted to the resonant triads? This cannot be done, because the resonant surfaces are complex enough for very accurate interpolation to be needed, rendering the resulting computation only relevant for a smooth distribution of the slow amplitudes a_s in Fourier space. Such a smooth distribution cannot represent turbulence, so that one has to resort to describing statistical quantities instead, which are naturally smooth. Closing the equations for these statistical moments renders a quasi-normal assumption necessary, yet resonant surface integrals can be employed, as described in the following section.

2.2. *Equations for second-order correlations*

From the definition of the second-order spectral tensor,

$$\langle\hat{u}_i(\boldsymbol{k},t)\hat{u}^*_j(\boldsymbol{p},t)\rangle=\Phi_{ij}(\boldsymbol{k},t)\delta(\boldsymbol{k}-\boldsymbol{p}), \quad (2.15)$$

and the relation (2.12) which links the fluctuating velocity and the slow-varying amplitudes, one may obtain the correlation tensor

$$\Phi_{ij}=\sum_{s,s'=\pm1}A_{ss'}(\boldsymbol{k},t)N_i(s\boldsymbol{k})N_j(s'\boldsymbol{k})\mathrm{e}^{\mathrm{i}(s+s')\sigma t} \quad (2.16)$$

where the $A_{ss'}$ are second-order correlations of the slow amplitudes

$$\langle a_s(\boldsymbol{k},t)a_{-s'}(\boldsymbol{k}',t)\rangle=A_{ss'}(\boldsymbol{k},t)\delta(\boldsymbol{k}+\boldsymbol{k}'). \quad (2.17)$$

These correlations are closely related to the set e, ζ, h (energy, polarization anisotropy, helicity, see Appendix B), as follows:

$$e = A_{1;-1} + A_{-1;1}, \qquad \zeta = 2A_{-1;-1}\mathrm{e}^{-2\mathrm{i}\sigma t}, \qquad h = A_{-1;1} - A_{1;-1}. \tag{2.18}$$

The following system of equations is obtained for the second-order spectral tensor:

$$\left(\frac{\partial}{\partial t} + 2\nu k^2\right) e = T^{(e)} = \frac{1}{2}(\tau_{ii} + \tau^*_{ii}), \tag{2.19}$$

$$\left(\frac{\partial}{\partial t} + 2\nu k^2 + 2\mathrm{i}\sigma_k\right) \zeta = T^{(\zeta)} = \frac{1}{2} N_i N_j (\tau_{ij} + \tau^*_{ji}), \tag{2.20}$$

$$\left(\frac{\partial}{\partial t} + 2\nu k^2\right) h = T^{(h)} = -\frac{1}{2}\mathrm{i}\frac{k_l}{k}\varepsilon_{lij}(\tau_{ij} + \tau^*_{ji}), \tag{2.21}$$

which may also be written for the $A_{ss'}$:

$$\frac{\partial A_{ss'}}{\partial t} = \frac{1}{4} N^*_i(s\boldsymbol{k}) N^*_j(s'\boldsymbol{k})(\tau_{ij} + \tau^*_{ji})\mathrm{e}^{-\mathrm{i}(s+s')\sigma t}. \tag{2.22}$$

Contributions from velocity triple correlations are collected into the symmetric generalized spectral transfer tensor $\tau_{ij} + \tau^*_{ji}$, which is an unclosed term in the equation that governs Φ_{ij}.

If the system of equations (2.19)–(2.21) start with three-dimensional isotropic initial data, that is with $e(k, t=0) = E(k)/(4\pi k^2)$ and $\zeta = h = 0$, $E(k)$ being a given distribution of spectral energy, anisotropy which reflects the transition towards two-dimensional structure may be created only by the nonlinear spectral transfer terms. This anisotropy has to be consistent with the axisymmetry of the problem, so that isotropy is broken through the dependence on $\theta = \cos^{-1}(k_\parallel/k)$ of the spectral quantities $e = e(k, \theta, t)$ and $\zeta = \zeta(k, \theta, t)$. Note that $\zeta(\boldsymbol{k})$ has to be zero when $\boldsymbol{k}$ is parallel to the vertical axis, if the closure model is to agree with the symmetries of the rotating Navier–Stokes equations (axisymmetry without mirror symmetry is ensured by the equations if initially satisfied).

2.3. *Improved EDQNM modelling from previous versions*

The derivation of a general quasi-normal (QN) model using the Green's function of the linear operator is detailed in Cambon & Scott (1999), and references therein. The corresponding expression for the tensor τ_{ij}, which reflects the contribution of triple correlations to the equation governing Φ_{ij}, consists of an integral over the third-order spectral tensor, the equation for which is closed by the quasi-normal relationship as follows:

$$\tau_{ij}(\boldsymbol{k}, t) = P_{jkl}(\boldsymbol{k}) \int_{-\infty}^{t} \int_{\boldsymbol{k}+\boldsymbol{p}+\boldsymbol{q}=0} G^{(0)}_{im}(\boldsymbol{k}, t, t') G^{(0)}_{kp}(\boldsymbol{p}, t, t') G^{(0)}_{lq}(\boldsymbol{q}, t, t') \times \Phi_{pn}(\boldsymbol{p}, t') \left[\tfrac{1}{2} P_{mnr}(\boldsymbol{k}) \Phi_{qr}(\boldsymbol{q}, t') + P_{qnr}(\boldsymbol{q}) \Phi_{mr}(\boldsymbol{k}, t')\right] \mathrm{d}^3\boldsymbol{p}\, \mathrm{d}t', \tag{2.23}$$

in which $P_{ijk}(\boldsymbol{k}) = k_j P_{ik}(\boldsymbol{k}) + k_k P_{ij}(\boldsymbol{k})$ and the viscous term is reinserted at no cost in the RDT Green's function as

$$G^{(0)}_{ij}(\boldsymbol{k}, t, t') = G^{RDT}_{ij}(\boldsymbol{k}, t, t')\mathrm{e}^{-\nu k^2 (t-t')}. \tag{2.24}$$

$\boldsymbol{G}^{(0)}$ directly generates the zeroth-order Kraichnan response function, which is a key quantity in any renormalized perturbation theory. The triple product of Green's functions in (2.23) arises from the Green's function solution of the third-order moment equation, and integration is performed over the triads such that $\boldsymbol{k} + \boldsymbol{p} + \boldsymbol{q} = \boldsymbol{0}$ so

that $\boldsymbol{q}$ should be replaced by $-\boldsymbol{k}-\boldsymbol{p}$ throughout the integrand. The only assumption in (2.23) is the quasi-normal writing of fourth-order velocity correlations in terms of products of second-order ones. The difference with quasi-isotropic versions is that the exact linear terms are taken into account, and anisotropy is explicitly retained in the formulation.

As in all renormalized perturbation theories, which were developed in isotropic turbulence, it is necessary to replace the 'bare' viscous Green's function (2.24) by a renormalized version, otherwise the resulting model is not realizable (Orszag 1970).

This is done in the eddy-damped quasi-normal model (EDQN) by changing the viscous factor νk^2 to $\mu = \nu k^2 + \mu'$ in the zeroth-order response function (2.24). Accordingly, the EDQN nonlinear transfer term is

$$\tau_{ij}(\boldsymbol{k},t) = P_{jkl}(\boldsymbol{k}) \int_{-\infty}^{t} \int_{\boldsymbol{k}+\boldsymbol{p}+\boldsymbol{q}=0} G_{im}(\boldsymbol{k},t,t') G_{kp}(\boldsymbol{p},t,t') G_{lq}(\boldsymbol{q},t,t') \times \Phi_{pn}(\boldsymbol{p},t') \left[\tfrac{1}{2} P_{mnr}(\boldsymbol{k}) \Phi_{qr}(\boldsymbol{q},t') + P_{qnr}(\boldsymbol{q}) \Phi_{mr}(\boldsymbol{k},t') \right] \mathrm{d}^3\boldsymbol{p}\, \mathrm{d}t', \quad (2.25)$$

with the mollified kernel

$$G_{ij}(\boldsymbol{k},t,t') = G_{ij}^{RDT}(\boldsymbol{k},t,t') e^{-\nu k^2 (t-t')} \exp\left(- \int_{t'}^{t} \mu'(k,t'')\, \mathrm{d}t'' \right). \quad (2.26)$$

The regularization coefficient $\mu'(k,t) = A(\int_0^k p^2 E(p,t)\mathrm{d}p)^{1/2}$ was proposed by Pouquet *et al.* (1975) for isotropic EDQNM. This eddy damping involves the inverse of the integral time scale introduced by Comte-Bellot & Corrsin (1971) instead of the local estimate $\mu' \sim k^{3/2} E^{1/2}$ initially proposed by Orszag (1970).

Equation (2.25) exhibits the generic anisotropic structure of most generalized classical theories dealing with two-point closure, or renormalized perturbation theories, but its zeroth-order limit involves, as the zeroth-order response tensor, a full RDT viscous Green's function which is more relevant than the laminar viscous one.

We now discuss the Markovianization procedure, i.e. the way we treat time-dependence in the integrands that connect the transfer term to second-order correlations. We notice three kinds of time-dependent terms in (2.25):

(*a*) viscous or viscous–damping terms $\exp(\int_{t'}^{t} \mu\, \mathrm{d}t'')$ which we write as $V(t,t')$,

(*b*) components of the RDT Green's function $\boldsymbol{G}(t,t')$, proportional to $\exp(\pm \mathrm{i}\sigma(t-t'))$,

(*c*) products of the second-order spectral tensor components $\Phi_{..}(t')$, or equivalent products of $e(t')$, $\zeta(t')$ and $h(t')$.

In the Markovianization procedure used in classical EDQNM$_1$, $V(t,t')$ is assumed to be rapidly decreasing in terms of the time separation $t-t'$ and the eddy–viscous damping μ varies slowly enough to be assumed constant. All the other terms are evaluated at $t'=t$ and are consistently replaced by $\boldsymbol{G}(t,t)$ and $\boldsymbol{\Phi}(t)$. However, since $\boldsymbol{G}(t-t')$ is responsible for breaking the initial isotropy in rotating turbulence, this model does not produce any anisotropic structure.

This drawback is removed in EDQNM$_2$ by approximating only the e, ζ and h terms at $t=t'$, and retaining the complete $V(t,t')$ and $G(t,t')$ terms in the time integrand. The latter integral of a three-fold product of response functions yields the following closed nonlinear transfer:

$$T^{(e,Z,h)} = \sum_{s=\pm1, s'=\pm1, s''=\pm1} \int \frac{S^{ss's''}(e,\zeta,h)}{\mu_{kpq} + \mathrm{i}(s\sigma_k + s'\sigma_p + s''\sigma_q)} \mathrm{d}^3\boldsymbol{p}. \quad (2.27)$$

EDQNM$_2$ compared well with high-resolution $528 \times 128 \times 128$ large-eddy simulations (LES) in view of the creation of directional anisotropy, and for predicting the development of anisotropy (CMG). However, regarding the rapid–slow decomposition (2.11), one can enlarge the scope of application of EDQNM$_2$ by relaxing the 'slow' approximation of e, ζ and h. In agreement with equation (2.18), only $Z = 2A_{-1;-1}$ has to be considered as a slow variable. In this EDQNM$_3$ model, $e(t') = e(t)$, $h(t') = h(t)$, $Z(t') = Z(t)$, but in the integral, $\zeta(t') = Z(t)\exp(-2\mathrm{i}\sigma t')$; and $V(t, t')$, $G(t, t')$ as before. This model consistently treats all $A_{ss'}$ as slow variables. EDQNM$_3$ differs only slightly from EDQNM$_2$, but offers valuable advantages. First, it is exactly equivalent to the model derived directly from the slow amplitudes, using (2.11) and (2.13). As a consequence, its asymptotic limit at large t, and small Rossby number, when $\mu \ll 2\Omega$, coincides exactly with Eulerian wave-turbulence theory. Second, realizability can be demonstrated in this limit (Bellet 2003), while it is not mathematically ensured in the EDQNM$_2$ version.

In EDQNM$_3$ the transfer tensor becomes

$$\begin{aligned}\tau_{ij}(\boldsymbol{k}, t) = \frac{1}{2} \sum_{s,s',s'',s_1,s_2} P_{jlm}(\boldsymbol{k}) \int_{\mathbb{R}^3} \int_{-\infty}^{t} \mathrm{e}^{[\mathrm{i}(s\sigma_k + s'\sigma_p + s''\sigma_q) - \mu_{kpq}](t-t')} \mathrm{e}^{\mathrm{i}(s'+s_1)\sigma_p t'} \\ \times N_i(s\boldsymbol{k}) N_l(s'\boldsymbol{p}) N_m(s''\boldsymbol{q}) N_k(s_1\boldsymbol{p}) A_{s's_1}(\boldsymbol{p}, t) \\ \times \left[\mathrm{e}^{\mathrm{i}(s''+s_2)\sigma_q t'} \tfrac{1}{2} P_{pkn}(\boldsymbol{k}) N_p(-s\boldsymbol{k}) N_n(s_2\boldsymbol{q}) A_{s''s_2}(\boldsymbol{q}, t)\right. \\ \left. + \mathrm{e}^{\mathrm{i}(s+s_2)\sigma_k t'} P_{pkn}(\boldsymbol{q}) N_p(-s''\boldsymbol{q}) N_n(s_2\boldsymbol{k}) A_{ss_2}(\boldsymbol{k}, t)\right] \mathrm{d}t' \mathrm{d}^3\boldsymbol{p} \end{aligned} \tag{2.28}$$

in which the quadratic slow amplitude terms have been set to their instantaneous values at t, and $\mu_{kpq} = \mu(k, t) + \mu(p, t) + \mu(q, t)$. Analytical time integration of exponential terms $\mathrm{e}^{\mathrm{i}(..)t'}$ is performed assuming constant μ, so that EDQNM$_3$ finally is

$$\begin{aligned}\tau_{ij}(\boldsymbol{k}, t) = \frac{1}{2} \sum_{s,s',s'',s_1,s_2} P_{jlm}(\boldsymbol{k}) \int_{\mathbb{R}^3} N_i(s\boldsymbol{k}) N_l(s'\boldsymbol{p}) N_m(s''\boldsymbol{q}) N_k(s_1\boldsymbol{p}) A_{s's_1}(\boldsymbol{p}, t) \\ \times \mathrm{e}^{\mathrm{i}(s'+s_1)\sigma_p t} \left[\tfrac{1}{2} P_{pkn}(\boldsymbol{k}) N_p(-s\boldsymbol{k}) N_n(s_2\boldsymbol{q}) \frac{A_{s''s_2}(\boldsymbol{q}, t)\mathrm{e}^{\mathrm{i}(s''+s_2)\sigma_q t}}{\mu_{kpq} - \mathrm{i}(s\sigma_k - s_1\sigma_p - s_2\sigma_q)}\right. \\ \left. + P_{pkn}(\boldsymbol{q}) N_p(-s''\boldsymbol{q}) N_n(s_2\boldsymbol{k}) \frac{A_{ss_2}(\boldsymbol{k}, t)\mathrm{e}^{\mathrm{i}(s+s_2)\sigma_k t}}{\mu_{kpq} - \mathrm{i}(s''\sigma_q - s_1\sigma_p - s_2\sigma_k)}\right] \mathrm{d}^3\boldsymbol{p}. \end{aligned} \tag{2.29}$$

The usual tensorial notation of the transfer is used in the above equation, but it is easy to derive corresponding equations for the sets $(A_{1;-1}, A_{-1;1}, A_{-1;-1})$ or (e, Z, h), as in CMG. The only difference between EDQNM$_2$ and EDQNM$_3$ concerns the rapid Coriolis-induced phase of ζ, or $s' = s_1$ and $s'' = s_2$ terms, so that the final EDQNM$_3$ expressions for (T^e, T^Z, T^h) are very close to those in CMG (also in the appendix of Cambon, Rubinstein & Godeferd 2004*b*, referred to herein as CRG).

Another way of obtaining these closed equations for the slow-amplitude double correlations is to construct moment equations in terms of $\langle a_s a_{s'}\rangle$, $\langle a_s a_{s'} a_{s''}\rangle$, etc., directly from equations (2.13) and (2.17). Since passing from $\hat{u}_i$ to a_s involves the eigenmodes N_i, as do the Green functions and projection operators, the amount of work is equivalent. The "Byzantine use of projectors" (Turner 1999), is not an impediment to deriving final equations in terms of slow amplitudes only, which is the aim of wave-turbulence Eulerian theory, as described in the following section.

3. The asymptotic quasi-normal Markovian (AQNM) model

3.1. *Removing rapid oscillations*

A simplified form of τ_{ij} is first obtained by taking t large, dropping those terms in equation (2.29) which are rapidly oscillating as functions of $\boldsymbol{p}$. Upon close examination of the corresponding terms in (2.29), this results in

$$\tau_{ij} = R_{ij} + \sum_{s_3,s_4=\pm 1} I_{ij;s_3s_4} A_{s_3s_4} \mathrm{e}^{\mathrm{i}(s_3+s_4)\sigma_k t} \tag{3.1}$$

where

$$R_{ij}(\boldsymbol{k},t) = \frac{1}{4}\sum_{s,s',s''} P_{jlm}(\boldsymbol{k})P_{pkn}(\boldsymbol{k})N_i(s\boldsymbol{k})N_p(-s\boldsymbol{k}) \times \int_{\mathbb{R}^3} N_k(-s'\boldsymbol{p})N_l(s'\boldsymbol{p})N_m(s''\boldsymbol{q})N_n(-s''\boldsymbol{q}) \frac{A_{s';-s'}(\boldsymbol{p},t)A_{s'';-s''}(\boldsymbol{q},t)}{\mu_{kpq} - \mathrm{i}[s\sigma(\boldsymbol{k}) + s'\sigma(\boldsymbol{p}) + s''\sigma(\boldsymbol{q})]} \mathrm{d}^3\boldsymbol{p},$$

which only involves the real components $A_{s;-s}(\boldsymbol{k},t)$ and

$$I_{ij;s_3s_4} = \frac{1}{2}\sum_{s',s''} P_{jlm}(\boldsymbol{k})N_i(s_3\boldsymbol{k})N_n(s_4\boldsymbol{k}) \times \int_{\mathbb{R}^3} N_k(-s'\boldsymbol{p})N_l(s'\boldsymbol{p})N_m(s''\boldsymbol{q})N_p(-s''\boldsymbol{q}) \frac{P_{pkn}(\boldsymbol{q})A_{s';-s'}(\boldsymbol{p},t)}{\mu_{kpq} - \mathrm{i}[s'\sigma(\boldsymbol{p}) + s''\sigma(\boldsymbol{q}) - s_4\sigma(\boldsymbol{k})]} \mathrm{d}^3\boldsymbol{p}. \tag{3.2}$$

Both R_{ij} and $I_{ij;s_3s_4}$ are slowly varying quantities, as is $A_{s_1s_2}$, so the above expression for τ_{ij} explicitly shows the fast-time dependence. Substituting the asymptotic result for τ_{ij} into the evolution equation for $A_{ss'}$ and dropping those terms which are rapidly oscillating in time, so that only terms with $s_3 + s_4 - s - s' = 0$ are conserved in equation (2.22), yields the equation

$$\frac{\partial A_{s;-s}}{\partial t} = B_s A_{s;-s} + C_s$$

with

$$B_s(\boldsymbol{k},t) = -2\sum_{s's''} \int_{\mathbb{R}^3} g_{s's''} \frac{\mu_{kpq}}{\mu_{kpq}^2 + F_{s's''}^2} A_{ss'}(\boldsymbol{p},t)\,\mathrm{d}^3\boldsymbol{p}, \tag{3.3}$$

$$C_s(\boldsymbol{k},t) = 2\sum_{s's''} \int_{\mathbb{R}^3} \gamma_{s's''} \frac{\mu_{kpq}}{\mu_{kpq}^2 + F_{s's''}^2} A_{ss'}(\boldsymbol{p},t)A_{ss''}(\boldsymbol{q},t)\,\mathrm{d}^3\boldsymbol{p}, \tag{3.4}$$

and the equation

$$\frac{\partial Z}{\partial t} = DZ, \qquad Z = 2A_{-1;-1}$$

with

$$D(\boldsymbol{k},t) = -\sum_{s's''} \int_{\mathbb{R}^3} g_{s's''} \frac{\mu_{kpq} + \mathrm{i}F_{s's''}}{\mu_{kpq}^2 + F_{s's''}^2} e(\boldsymbol{p},t)\,\mathrm{d}^3\boldsymbol{p}. \tag{3.5}$$

The expression for $\gamma_{s's''}$ is given in the next section in terms of $g_{s's''}$, itself detailed in Appendix D in terms of (k, p, q). Again, as in EDQNM$_2$, dispersion frequencies appear only through the term $F_{s's''} = \sigma_k + s'\sigma_p + s''\sigma_q$.

3.2. *The asymptotic limit of small damping*

The asymptotic evolution equations are obtained by taking the limit $\mu_{kpq} \to 0$ in the above expressions for C_s, B_s and D. In wave-turbulence theory, it is usual to replace the volume integral by a surface integral over the resonant surface in this limit, for instance, the Plemelj–Sokhotsky formula $1/(d - \mathrm{i}x) = \pi\delta(x) + \mathrm{i}\mathscr{P}(1/x)$ is used by Caillol & Zeitlin (2000), where $\mathscr{P}$ is the principal value. However, taking the limit is not simple, and is valid only for the real part of the rational fraction involved in equation (3.5) or in equations (3.3) and (3.4), but not for the imaginary part of the fraction appearing in the D coefficient. In this section, we briefly present the path to the final surface integrals, taking the limits for granted. Details on their derivation are given in Appendix C.

Starting with the real part, it is necessary to parameterize the resonant surface, which is the set

$$S_{s's''}(\boldsymbol{k}) = \{\boldsymbol{p} \in \mathbb{R}^3, \quad \text{such that} \quad \sigma(\boldsymbol{k}) + s'\sigma(\boldsymbol{p}) + s''\sigma(-\boldsymbol{k} - \boldsymbol{p}) = 0\}. \tag{3.6}$$

We also introduce the parameter d which plays the role of μ_{kpq} in the above. Knowing the following limit of the function of x:

$$f_d(x) = \frac{d}{d^2 + x^2} \to \pi\delta(x) \quad \text{for} \quad d \to 0,$$

one finds that

$$\int_{\mathbb{R}^3} A(\boldsymbol{k}, \boldsymbol{p}) \frac{d}{d^2 + F_{s's''}^2} \,\mathrm{d}^3\boldsymbol{p} \to \pi \int_{\mathbb{R}^3} \delta(F_{s's''}) A(\boldsymbol{k}, \boldsymbol{p}) \,\mathrm{d}^3\boldsymbol{p} \tag{3.7}$$

when d goes to zero. The latter integral is recast as the surface integral

$$\int_{S_{s's''}} \frac{A(\boldsymbol{k}, \boldsymbol{p})}{\alpha_{s's''}} \,\mathrm{d}S$$

in which $\alpha_{s's''}$ denotes the gradient of the function $F_{s's''}/\pi$ along the direction normal to the surface $F_{s's''} = 0$:

$$\alpha_{s's''} = \frac{1}{\pi} |s'\boldsymbol{C}_g(\boldsymbol{p}) - s''\boldsymbol{C}_g(\boldsymbol{q})|.$$

The coefficient $\alpha_{s's''}$ involves the group velocity $\boldsymbol{C}_g(\boldsymbol{k}) = -(2\Omega k_\perp/k^2)\boldsymbol{e}^{(2)}(\boldsymbol{k})$ and is therefore angular dependent.

For the imaginary part of the fraction in equation (3.5) for D, one uses the limit at vanishing d:

$$\int_{\mathbb{R}^3} \frac{F_{s's''}}{d^2 + F_{s's''}^2} A(\boldsymbol{k}, \boldsymbol{p}) \,\mathrm{d}^3\boldsymbol{p} \to \fint_{\mathbb{R}^3} \frac{A(\boldsymbol{k}, \boldsymbol{p})}{F_{s's''}} \,\mathrm{d}^3\boldsymbol{p} \tag{3.8}$$

which is a principal value integral in the vicinity of the resonant surface.

Accordingly, the coefficients B_s, C_s, D take the following asymptotic values, in the limit of vanishing μ_{kpq}:

$$B_s(\boldsymbol{k}, t) = -2 \sum_{s', s''} \int_{S_{s's''}} \frac{g_{s's''}}{\alpha_{s's''}} A_{ss'}(\boldsymbol{p}, t) \,\mathrm{d}S, \tag{3.9}$$

$$C_s(\boldsymbol{k}, t) = 2 \sum_{s's''} \int_{S_{s's''}} \frac{\gamma_{s's''}}{\alpha_{s's''}} A_{ss'}(\boldsymbol{p}, t) A_{ss''}(\boldsymbol{q}, t) \,\mathrm{d}S, \tag{3.10}$$

$$D(\boldsymbol{k},t) = -\sum_{s',s''}\left[\int_{S_{s's''}} \frac{g_{s's''}}{\alpha_{s's''}} e(\boldsymbol{p},t)\,\mathrm{d}S + \mathrm{i}\!\!\int_{\mathbb{R}^3} \frac{g_{s's''}}{F_{s's''}} e(\boldsymbol{p},t)\,\mathrm{d}^3\boldsymbol{p}\right]. \tag{3.11}$$

Going back to variables e, Z, h from their definitions (2.18) one finds (omitting the obvious explicit time dependence of the spectra)

$$T^{(e)} = \sum_{s's''}\int_{S_{s's''}} \frac{g_{s's''}}{\alpha_{s's''}}[e(\boldsymbol{p})(e(\boldsymbol{q})-e(\boldsymbol{k})) + s'h(\boldsymbol{p})(s''h(\boldsymbol{q})-h(\boldsymbol{k}))]\,\mathrm{d}S,$$

$$T^{(h)} = \sum_{s's''}\int_{S_{s's''}} \frac{g_{s's''}}{\alpha_{s's''}}[s'h(\boldsymbol{p})(e(\boldsymbol{q})-e(\boldsymbol{k})) + e(\boldsymbol{p})(s''h(\boldsymbol{q})-h(\boldsymbol{k}))]\,\mathrm{d}S,$$

and $T^{(Z)} = ZD(\boldsymbol{k},t)$, using $\gamma_{s's''}(\boldsymbol{k},\boldsymbol{p},\boldsymbol{q}) = [g_{s's''}(\boldsymbol{k},\boldsymbol{p},\boldsymbol{q}) + g_{s''s'}(\boldsymbol{k},\boldsymbol{q},\boldsymbol{p})]/2$ in (3.10). In addition to the gradient term $\alpha_{s's''}$, these transfer integrals only involve a single geometric factor $g_{s's''}$ given in equation (D 2).

3.3. *Preliminary comments about AQNM final equations*

The transfer terms $T^{(e)}$ and $T^{(h)}$ exactly set the rates of change $\partial e/\partial t$ and $\partial h/\partial t$ in the inviscid limit. They look similar to those derived by Galtier (2003), but geometric coefficients may differ, according to the way integrands are symmetrized in terms of $\boldsymbol{p}$ and $\boldsymbol{q}$. Although a non-zero viscous–damping coefficient $d = \mu_{kpq}$ has to be considered in order to correctly derive the asymptotic limit, this d term no longer appears in the final equations.

Strong anisotropy results from the angular-dependent $\alpha_{s's''}$ term and from the topology of the resonant surfaces themselves; both effects reflect the appearance of a Dirac function $\delta(F_{s's''})$ in energy and helicity transfers (see also Galtier 2003). Because of the link of $\alpha_{s's''}$ to the group velocity, the transfers scale as $1/\Omega$, which therefore replaces the eddy-damping time scale $1/\mu_{kpq}$ in classical EDQNM models with no rotation.

In the strict limit $\cos\theta = 0$, the resonant surfaces approach the horizontal plane and a vertical plane, so that only planar triads are involved for e and h, as in pure two-dimensional turbulence. This result is consistent with the first-order decoupling of the purely two-dimensional mode observed by Waleffe (1993). Nevertheless, we have seen that the AQNM energy transfer always scales as $1/\Omega$, whereas the rotation term disappears in the purely two-dimensional case. In addition, the geometric coefficient $g_{s's''}/\alpha_{s's''}$ in AQNM at $\cos\theta = 0$ does not coincide with its counterpart in, e.g., two-dimensional EDQNM (Leith 1971).

The transfer $T^{(Z)}$ in AQNM is linear in Z, and is the only term which does not reduce to a surface integral. Much more complex quadratic interaction terms that involve Z in volumic EDQNM_{2-3} models are discarded in AQNM when removing rapidly oscillating terms. The latter approximations, used in § 3.1, are valid if $\mathrm{e}^{\mathrm{i}\alpha\sigma_k t}$ with $\alpha = s_3 + s_4 - s - s' = \pm 2, \pm 4$ are very rapidly oscillating terms. They are questionable if $\cos\theta = k_\parallel/k$ is small enough, with a value of the same order as the inverse of the rotation frequency, since $\sigma_k = 2\Omega\cos\theta_k$. Accordingly, there exists a domain in which AQNM equations are no longer valid. As a consequence, the $A_{ss'}$ have to be governed by different equations in the inner 'slow manifold' and in the outer domain; hence these 'slow amplitudes' can vary rapidly in the vicinity of $k_\parallel = 0$, so that the slow/fast time separation is no longer valid and the resonance condition does not hold for the 'slow' manifold. This issue is further discussed in § 6.2 and in CRG.

4. Numerical scheme for the energy equation

From the previously introduced dynamical equations, we retain only the energy equation e, since we take $h = Z = 0$ initially, and the equations for h and Z imply that they remain zero. The following Lin-type equation has to be solved:

$$\frac{\partial e}{\partial t} + 2\nu k^2 e = \sum_{s's''} \int_{S_{s's''}} \frac{g_{s's''}(k, p, q)}{\alpha_{s's''}(\boldsymbol{p}, \boldsymbol{q})} e(\boldsymbol{p}, t)[e(\boldsymbol{q}, t) - e(\boldsymbol{k}, t)]\, \mathrm{d}^2 \boldsymbol{p}. \tag{4.1}$$

This equation is dimensional, and its dimensional analysis, with related definitions of key non-dimensional time scales, can be obtained as follows. The wavenumber is non-dimensionalized by K_0, which is an inverse length scale; the energy spectrum e is scaled by an energy density amplitude A. A typical velocity scale is $u' \sim A^{1/2} K_0^{3/2}$; instead of defining a typical time scale by $L/u' \sim A^{-1/2} K_0^{-5/2}$, the scaling of the nonlinear time scale derives from the scaling of equation (4.1). The ratio $g_{s's''}/\alpha_{s's''}$ scales as $\pi K_0^3/\Omega$, so that the transfer term can be evaluated by $T^{(e)} \sim \pi K_0^5 A^2/\Omega$, and from $e_{,t} \sim A/\hat{t}_{NL} \sim \pi(K_0^5/\Omega)A^2$ the typical nonlinear time scale is derived:

$$\hat{t}_{NL} = \frac{\Omega}{\pi A K_0^5}.$$

On the other hand, a classical Rossby number is defined as $Ro \sim u'/(\Omega L)$ or

$$Ro = A^{1/2} K_0^{5/2} \Omega^{-1},$$

so that $\Omega t \sim Ro^{-2}$ for $t \sim \hat{t}_{NL}$. Thus, the evolution time for e implied by (4.1) is $O(Ro^{-2}\Omega^{-1})$.

One can distinguish three domains, depending on the elapsed time. At the shortest times, $\Omega t \sim 1$, nonlinearity is negligible, and e is conserved. At larger times, $\Omega t \sim Ro^{-1}$, one recovers the time scale which is relevant for classical nonlinear dynamics, e.g. related to conventional energy transfer in terms of volume integral. Only at the largest times, $\Omega t \sim Ro^{-2}$, can the 'weak' cascade become established in inertial wave-turbulence, and e evolve.

The previous analysis is essentially inviscid. If the viscous term is accounted for in equation (4.1), only for numerical convenience, a fictitious Reynolds number can be defined as $Re = \pi A k_0^3/(2\Omega\nu)$. Since the typical time scaling $t/\hat{t}_{NL}$ is used, the Rossby number has disappeared at this point, and an apparently low value of the Reynolds number is found.

Starting from a pure three-dimensional isotropic case, with $e = E(k)/4\pi k^2$, an angular-dependent $e(k, \theta, t)$ distribution is created by the anisotropic energy transfer. The viscous term is marginal in our study since we are interested in the limit of infinite Reynolds number and vanishing Rossby number. Non-zero viscosity will be introduced only for numerical convenience. Since we have used an Euler scheme for time marching, the viscous term in (4.1) can be readily added in an implicit way by using integrating factors.

Numerical implementation, parameters

First of all, from equation (4.1) we note that if the energy spectrum is initially axisymmetric or contains mirror symmetry, it conserves this property. This is used for reducing the number of degrees of freedom in the computation. Singularities due to the cancelling of the denominator $\alpha_{s's''}$ are removed by using symmetries of the integrand (see Bellet 2003 for details).

The integral in (4.1) can be recast in terms of the normalized wavevectors $\boldsymbol{K} = \boldsymbol{k}/k$, $\boldsymbol{P} = \boldsymbol{p}/k$ and $\boldsymbol{Q} = \boldsymbol{q}/k$. Without loss of generality the components of $\boldsymbol{K}$ are

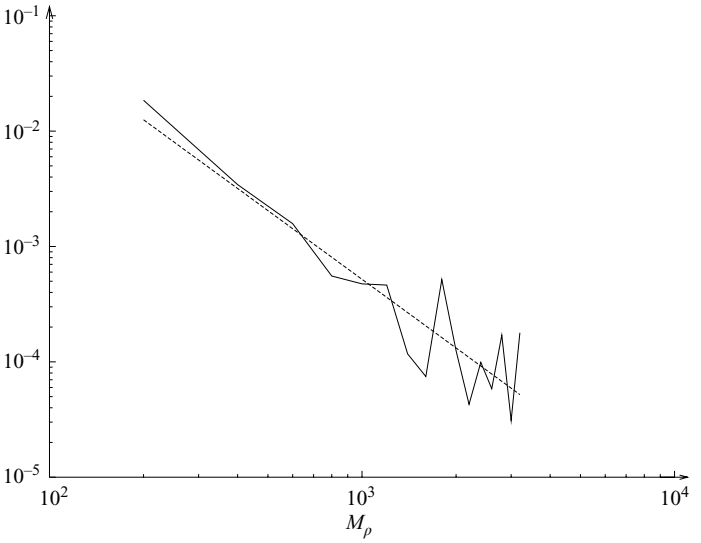

FIGURE 1. ———, Variation of the unsigned value of the integrated transfer as a function of M_ρ, with $M_\theta = 200$, $M_\phi = 100$, $k_m = 0.1$ and $k_{max} = 10$. – – – –, The least-squares fit, exhibiting a $M_\rho^{-1.98}$ dependence.

$K_1 = \sin\theta$, $K_2 = 0$, $K_3 = \cos\theta$. The second leg of the triad is parameterized in spherical coordinates with an exponential radius as $\boldsymbol{P} = \exp(\rho)[\sin\theta'\cos\phi', \sin\theta'\sin\phi', \cos\theta']$, and $\boldsymbol{Q}$ is the difference $\boldsymbol{K} - \boldsymbol{Q}$. The choice of an exponential radial parameter simplifies the computation of the geometric coefficients. In view of the symmetries of the integral, the triplet is such that $\rho \in]-\infty, \infty[$, $\theta' \in]0, \pi[$ and $\phi' \in]0, \pi[$.

This parameter space for $\boldsymbol{P}$ is discretized using M_ρ values for ρ (which yield $P \in [k_m, k_M]$), M_θ polar angles and M_ϕ azimuthal ones. The intersection of each elementary volume of this grid with the surface $S_{s's''}$ is obtained by inspection of the sign of the characteristic function $f_{s's''}(\rho, \theta', \phi') = \cos\theta + s'P_3/P + s''Q_3/Q$ over each vertex of the elementary volume cell. A change of sign indicates that the resonant surface intersects the cell, and the contributed area is computed by a first-order estimate, assimilating the surface locally to a plane. This allows one to compute the geometrical coefficients in the energy integral of (4.1). Knowing the numerical values of the energy e at the preceding time step over the grid points, one still has to obtain the energy for $\boldsymbol{Q}$, which do not necessarily lie on the grid. The required $e(\boldsymbol{Q})$ is interpolated with a two-dimensional second-order scheme using the values at neighbouring points.

Choosing values for M_ρ, M_θ and M_ϕ is not easy, and we start with the value 100 for each and let them vary to check the effects of discretization (see Appendix E for details). We then study the dependence of the numerically integrated energy transfer, which should cancel out over the whole spectral space due to energy conservation:

$$\int_0^\infty k^2 \left(\int_0^\pi T(k, \theta) \sin\theta \, \mathrm{d}\theta \right) \mathrm{d}k = 0.$$

Of course, the above integral is not exactly zero for a finite discretization and truncated k, but should be small, and converge to zero with increasing degrees of freedom. The dependence on M_ρ is the strongest, which we estimate to be with a power between one and two, as illustrated by figure 1.

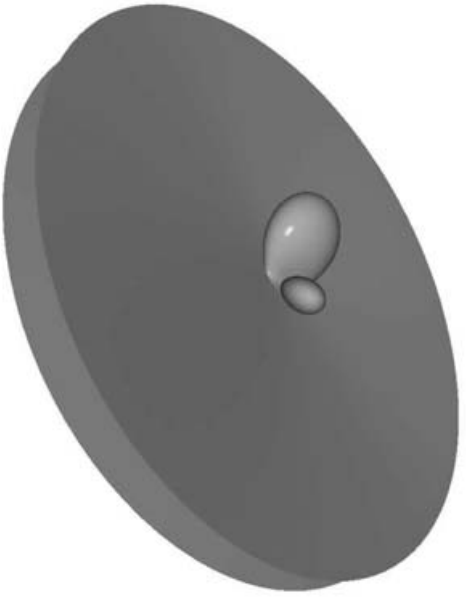

FIGURE 2. Three-dimensional rendering of the resonant surface, i.e. the locus of $\boldsymbol{p}$, at $k = 1$ and $\theta_k = 1.4$, with 100 points of discretization for wavenumbers, latitude and azimuthal angles. The large conical-shaped fold is theoretically infinite, but is truncated at the maximum wavenumber. Two smaller closed folds are observed on top of it. The same symmetrical folds exist behind these, only hinted here. Note that the points connecting the closed folds and the infinite one are singular and quite complex to accurately account for.

A three-dimensional plot of a resonant surface for $\theta = 1.4$ is provided in figure 2, showing how complex resonant surfaces can become, exhibiting cusps at the connection of the different folds. When θ varies between 0 and $\pi/2$, the surface shape changes, the closed loops eventually becoming infinite.

5. Numerical results

Solving numerically the AQNM energy equation reliably with accuracy has been the main challenge of this study. To our knowledge, this has never been done in the wave-turbulence community. Given the complexity of resonant surfaces, numerical integration has to involve a huge number of degrees of freedom; related matrices have a typical size, for instance 300^3 at the maximum, which can be of the same order of magnitude as for pseudo-spectral DNS. The important computational resources used to solve the AQNM energy equation were also used to perform new runs of the volumic EDQNM2-3 code, with much better conditions (spatial resolution, number of time steps) than in any previous computation.

In contrast to the numerical cost of a single typical AQNM run, the parametric study is dramatically reduced. Since AQNM addresses the asymptotic limit of vanishing Rossby number, there is no need for different values of the Rossby number. The limit of an infinite Reynolds number is mainly addressed too, and viscosity is reintroduced only for numerical convenience, yielding very few different runs for different Reynolds numbers.

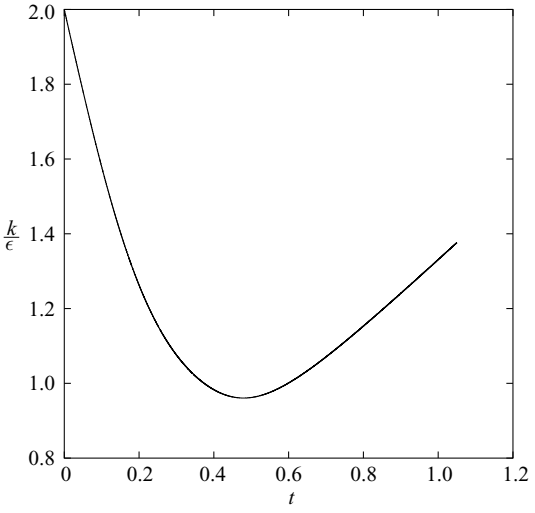

FIGURE 3. Ratio k/ϵ as a function of time.

5.1. *Time evolution of the energy and related transfer*

AQNM equation (4.1) is solved starting from an isotropic narrow-band energy spectrum, as is usual in DNS and EDQNM (Orszag 1969). During a first phase, without viscosity, an inertial zone develops, and extends towards larger and larger wavenumbers. At a time $t_f(k_{max})$, the inertial zone reaches the largest wavenumber of the mesh, denoted k_{max}, and the tail of the energy spectrum begin to display a bump, which can eventually create a numerical instability. A laminar viscous term is added to remove this bump, and to allow us to continue the calculation to larger times. In this sense, viscosity is a numerical artifact, and the low value of the typical Reynolds numbers defined below is not physically relevant. The ratio of kinetic energy to dissipation, k/ϵ, is plotted on figure 3 as a function of time. In isotropic turbulence, it is expected to evolve linearly with time after the initial transient, and this behaviour is recovered here as shown on figure 3.

5.1.1. *Distribution of the spectral density of energy and related transfer*

We first consider the energy spectrum $E(k,t)$ which is derived from $e(k,\cos\theta,t)$ by spherical integration over θ of the energy density spectrum:

$$E(k,t) = 4\pi k^2 \int_0^1 e(k,x,t)\,\mathrm{d}x, \qquad x = \cos\theta.$$

Figure 4 shows the evolution of $E(k)$ starting from the narrow-band spectrum we have selected as the initial condition. There are two stages in the time evolution of the spectrum. First, as shown on figure 4(a), the spectrum widens until it reaches the smallest scales consistent with the dynamics at the given Reynolds number $Re = 5$. The corresponding time is approximately $t = 0.525$. At this point, the dissipative subrange is completely operative, and the spectrum begins to decay so that the system globally loses energy, as shown in figure 4(b). As the first notable result, the inertial range is established naturally with a clear k^{-3} power law for $E(k)$. This scaling of the inertial range was identified in rotating turbulence in forced numerical simulations by e.g. Smith & Waleffe (1999); Hossain (1994), recovered in high-resolution freely

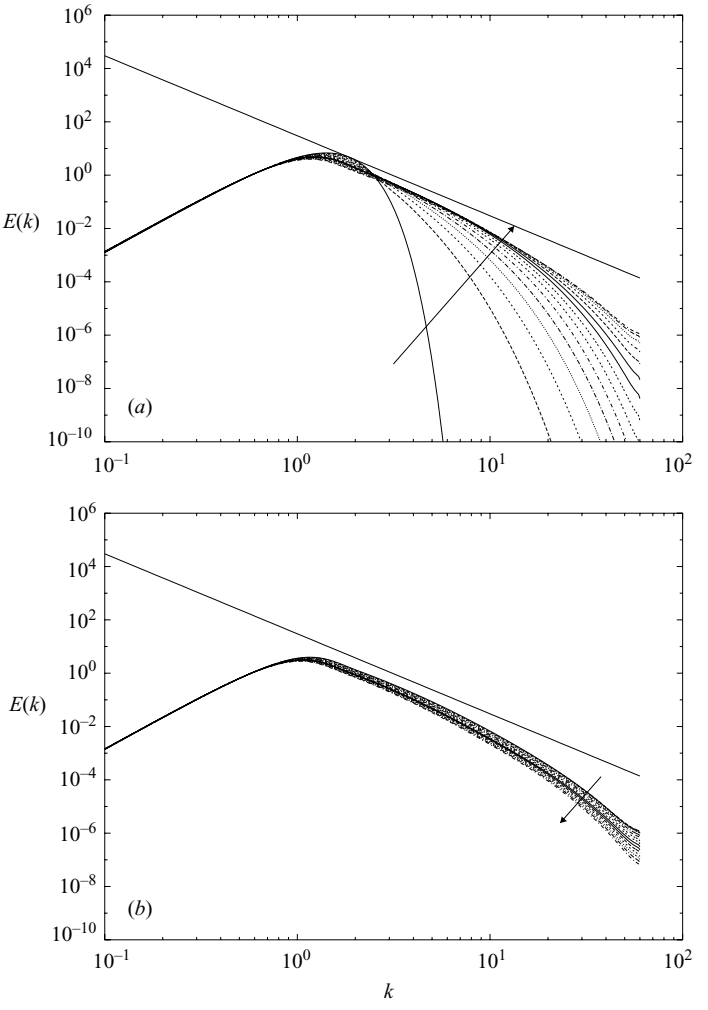

FIGURE 4. Temporal evolution of the spherically integrated energy spectrum at $Re = 5$, $k_{\max} = 60$, $\mathrm{d}t = 5 \times 10^{-5}$: (*a*) between $t_0 = 0$ and $t = 0.525$ in steps of 0.0375; (*b*) between $t = 0.525$ and $t_f = 1.05$ with the same time step. The arrows denote increasing time and the straight line shows the k^{-3} dependence.

decaying EDQNM$_{2,3}$ with the highest resolution (Bellet 2003), and in LES by Yang & Domaradzki (2004).

The build-up of the angular dependence is illustrated by iso-values of e in the (k, θ)-plane, plotted in figure 5. The initial distribution (shown on figure 5*a*) is isotropic, so that the contours are straight lines parallel to the θ-axis, showing no dependence of the spectrum on the angle θ. Almost instantaneously after $t = 0$ (figure 5*b*), the spectrum begins to spread in the angular direction, showing an exchange of energy between different inertial waves of different propagation angle, as an adjustment of the dynamics of turbulence under the effect of the Coriolis force. Of course, energy is also transferred between different wavenumbers, as observed in figures 5(*c*) to 5(*e*), at which point the angular equilibrium of the spectrum is almost reached. Finally, the last figure 5(*f*) shows that e is large in the neighbourhood of the horizontal plane

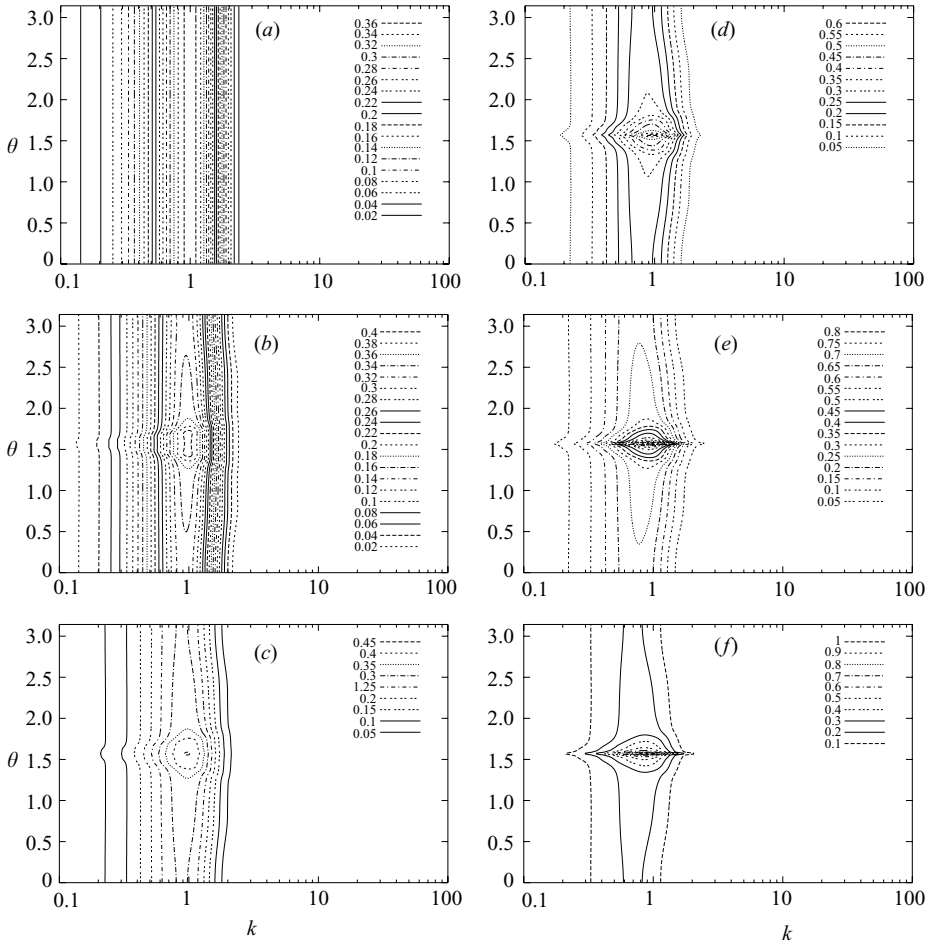

FIGURE 5. Iso-values of the spectral energy density $e(k,\theta)$ at $Re=5$, $k_{max}=60$, $\mathrm{d}t=5\times10^{-5}$ between $t=0$ and $t=0.75$: (*a*) $t=0$, (*b*) 0.075, (*c*) 0.15, (*d*) 0.3, (*e*) 0.45, (*f*) 0.75.

$\theta=\pi/2$, whereas only a weak angular dependence of the energy density spectrum is observed away from this region. This distribution is qualitatively very similar to the one found by CMG (their figure 6), both from EDQNM$_2$ results and large-eddy simulation of homogeneous turbulence with rotation.

An additional viewpoint on the energy density distribution is obtained by plotting the compensated spectrum $4\pi k^2 e(k,\cos\theta,t)$ versus k, at different fixed angles θ as done on figures 6(*a*) and 6(*b*). All curves collapse onto $E(k)$ for isotropic turbulence (e.g. here at $t=0$). For angles close to $\pi/2$, the slopes are significantly less steep than k^{-3}, about k^{-2}, whereas they are steeper than k^{-3} for angles far from $\pi/2$. It is therefore clear that the k^{-3} law for $E(k,t)$ results from averaging over all angles. Figures 6(*c*) and 6(*d*) represent the same quantity multiplied by $\sin\theta$, which is the weighting factor which appears in the integral when computing $E(k,t)$. Figures 6(*a*, *c*) shows the distribution at $t=0.525$ and (*b*, *d*) at $t=1.05$, from which we notice that the level of the spectrum that is close to horizontal has increased between these times.

Comparing either figures 6(*a*) and 6(*b*) or 6(*c*) and 6(*d*) indicates a striking similarity between the spectra at different times. More detailed study shows that, leaving aside

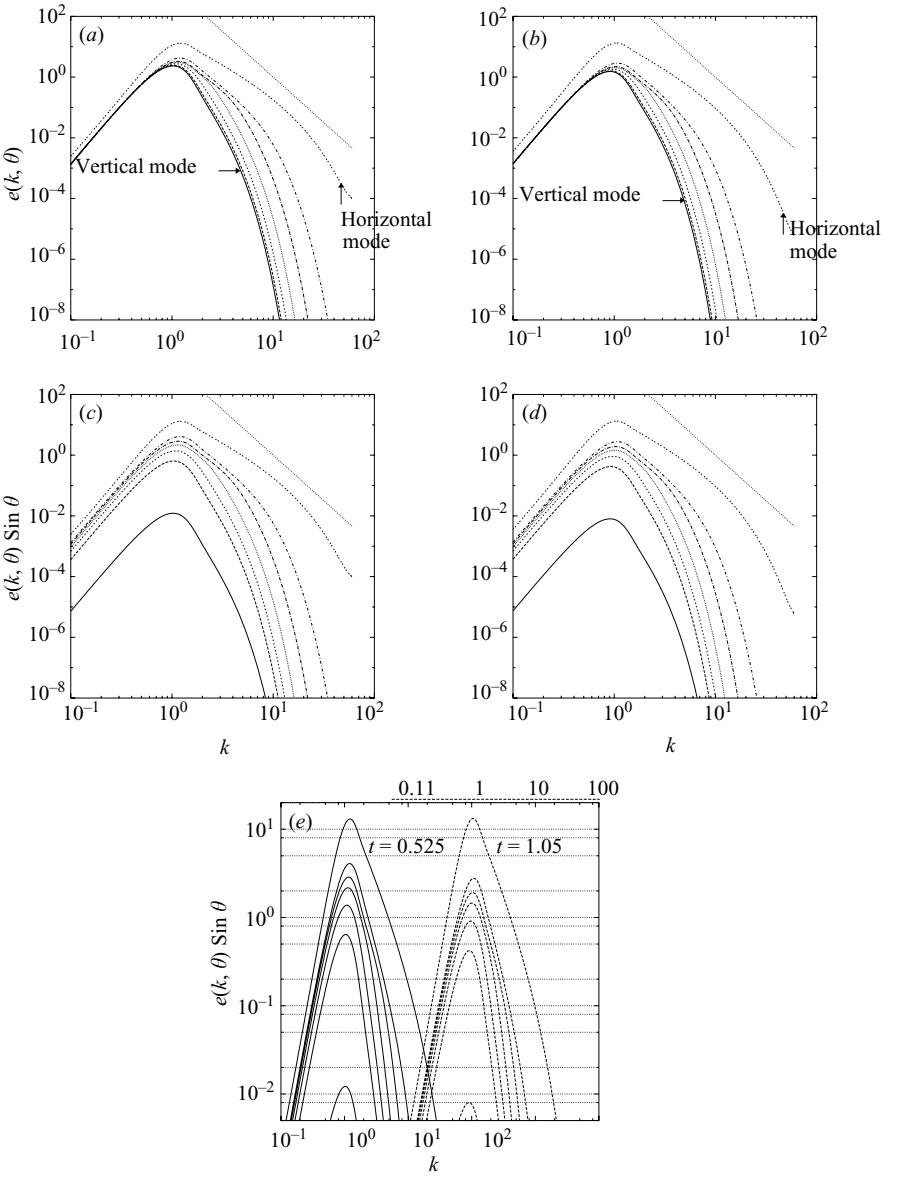

FIGURE 6. Spectral energy density for different angles, from bottom to top, $\theta/(\pi/2) = 1/300$ (what we call the 'vertical' mode, 51/300, 101/300, 151/300, 201/300, 251/300 and 299/300 (the 'horizontal' mode) at $Re = 5$, $k_{\max} = 60$, $\mathrm{d}t = 5 \times 10^{-5}$, at (a) $t = 0.525$ and (b) $t = 1.05$. (c, d) The same quantity multiplied by the corresponding $\sin\theta$ for each given angle. The k^{-3} slope is also plotted. (e) Same as (c) and (d) with a zoomed scale and data at $t = 1.05$ shifted two decades to the right (axis labels on top).

the high-wavenumber components which are affected by viscosity and the highest of the curves (very nearly horizontal wavectors), spectral evolution is self-similar. This is best observed in figure 6(e) which combines plots 6(c) and 6(d) on a zoomed scale. Whereas the maximum energy density for the angle close to the horizontal hardly changes, the remaining curves fall together with increasing time. It therefore appears

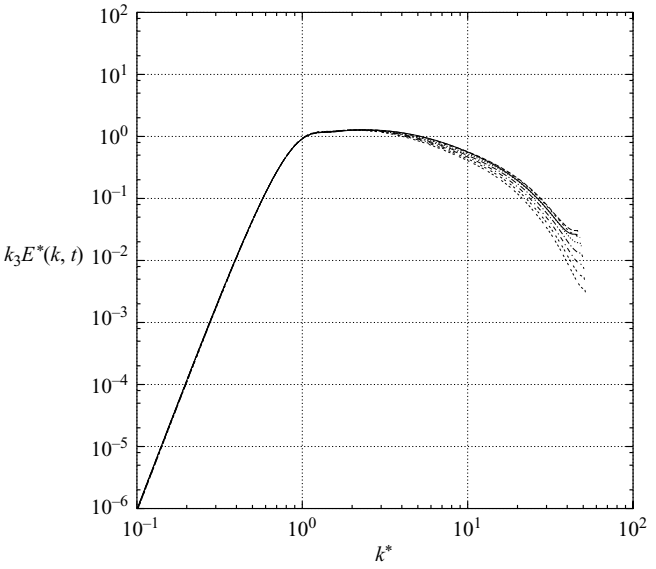

FIGURE 7. Self-similarity of the spherically integrated energy spectra multiplied by k^3 at times t between 0.525 and 1.05, renormalized by the time-dependent total kinetic energy, plotted as a function of the wavenumber k^*, renormalized by the time-dependent peak wavenumber.

that the large-time behaviour is self-similar outside a neighbourhood of $\theta = \pi/2$ whose width decreases to zero. Figure 7 confirms this conclusion.

In isotropic turbulence, the direction over which spectra are integrated in spectral space to yield one-dimensional spectra does not modify the $k^{-5/3}$ power law of the inertial range. However, the same integration of the anisotropic spectrum $e(k, \cos\theta)$ over horizontal planes in spectral space, or over vertical cylinders, modifies the scaling of the resulting one-dimensional spectrum, as exhibited on figures 8(a) and 8(b) respectively. In the one-dimensional horizontal spectra $E_h(k_\parallel)$ and $E_h(k_\perp)$, the scaling is not k^{-3} whereas this scaling describes the vertical spectra $E_v(k_\parallel)$ and $E_v(k_\perp)$. This is due to the specific distribution in spectral space directions of the energy density spectrum $e(k, \cos\theta)$.

A way of quantifying the angular distribution of energy is to compute the energy at each angle integrated over every wavenumber

$$E_{\mathrm{ang}}(\theta, t) = 2\pi \int_0^\infty k^2 e(k, \theta, t)\, \mathrm{d}k \tag{5.1}$$

such that the total energy is recovered as $E_t(t) = \int_0^\pi E_{\mathrm{ang}}(\theta, t) \sin\theta\, \mathrm{d}\theta$. Another interesting quantity is the fraction of the total energy contributed by angles between θ and $\pi - \theta$:

$$E_{\mathrm{frac}}(\theta, t) = E_t^{-1} \int_\theta^{\pi-\theta} E_{\mathrm{ang}}(\theta, t) \sin\theta\, \mathrm{d}\theta. \tag{5.2}$$

The two quantities E_{ang} and E_{frac} are plotted in figure 9. Their time evolution is shown, starting with isotropic initial conditions, for which $E_{\mathrm{ang}}(\theta) = E_t/2$ and $E_{\mathrm{frac}} = \cos\theta$. Figure 9($a$) shows that E_{ang} grows rapidly for θ close to $\pi/2$, developing a sharp peak for horizontal wavevectors and a distribution which is far from isotropic at the end of the computation. Figure 9(b) also shows the development of anisotropy

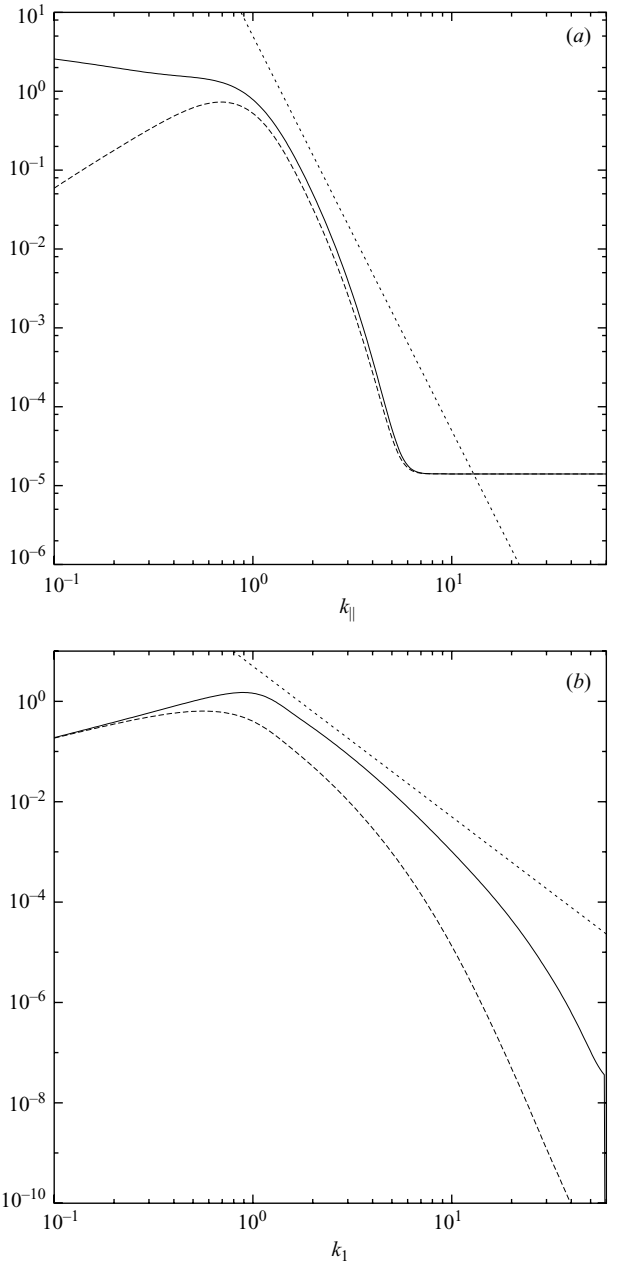

FIGURE 8. (*a*) One-dimensional spectra $E_{h,v}(k_{\|})$ integrated on planes as a function of the vertical wavenumber component $k_{\|}$; (*b*) one-dimensional spectra $E_{h,v}(k_{\perp})$ integrated over cylinders as a function of the horizontal wavenumber $k_{\perp}$, at $Re = 5$, $k_{\max} = 60$, $\mathrm{d}t = 5 \times 10^{-5}$ at $t = 1.05$. Solid lines show the horizontal correlation spectrum E_h, and dashed lines the vertical correlation spectrum E_v. Straight lines show: (*a*) k^{-5} power law; (*b*) k^{-3} power law.

and that $E_{\mathrm{frac}}(\theta, t)$ appears to approach a limit $E^{\infty}_{\mathrm{frac}}(\theta)$ at large times, reflecting the self-similarity discussed earlier. According to these results, 50 % of the energy at the end of the run is contained between $\theta = 0$ and $\theta = 1.25$. Taken together, figures 9(*a*) and 9(*b*) indicate that, although E_{ang} appears to develop an infinite singularity

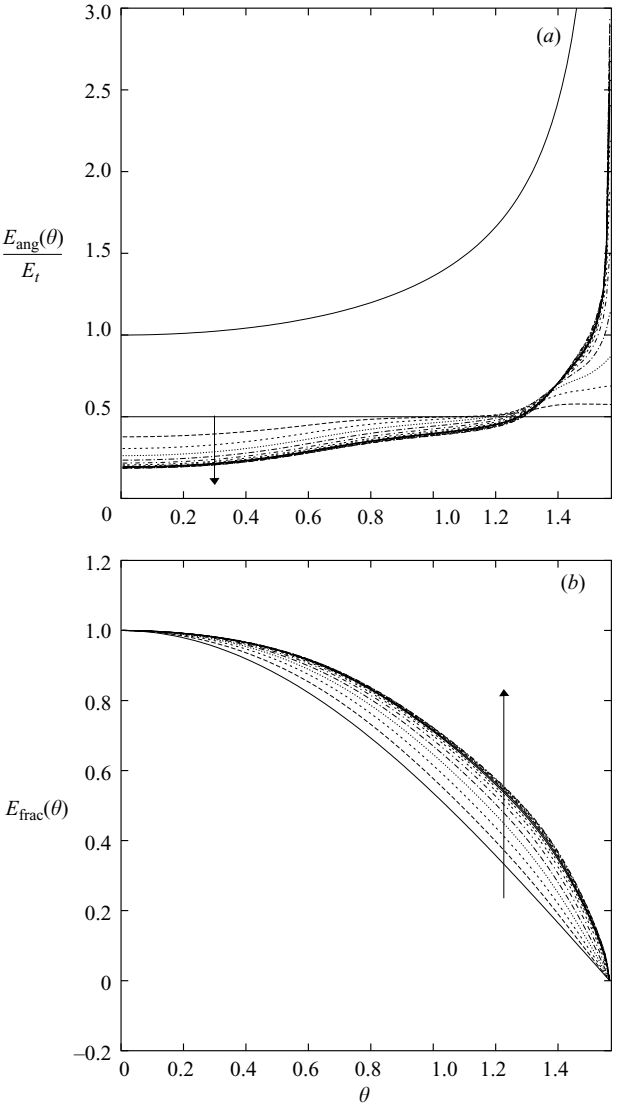

FIGURE 9. Time evolution of (*a*) $E_{ang}(\theta)/E_t$ at $Re = 5$, $k_{max} = 60$, $dt = 5 \times 10^{-5}$, between $t = 0$ and $t = 1.05$. (The uppermost solid line shows a $1/\sqrt{\cos\theta}$ dependence.) (*b*) $E_{frac}(\theta)$ for the same set of parameters.

at $\theta = \pi/2$, this singularity is integrable and hence does not dominate the overall energy.

In the same way as these angular-dependent quantities have been defined for the energy, one may compute a similar function from the energy transfer spectrum, the time evolution of which is plotted on figure 10, by merely replacing $e(\theta, k, t)$ by $T(\theta, k, t)$ in equation (5.1), thus yielding $T_{ang}(\theta, t)$. From this quantity, one obtains the energy flux across a cut at θ: $E_{flux}(\theta, t) = \int_{\theta}^{\pi/2} T_{ang}(\theta, t) \sin\theta \, d\theta$. Figure 11 shows how this quantity evolves in time: the energy flux is maximal at the beginning of the computation, but its maximum is shifted as time increases towards the horizontal plane $\theta = \pi/2$, reaching almost 1.5.

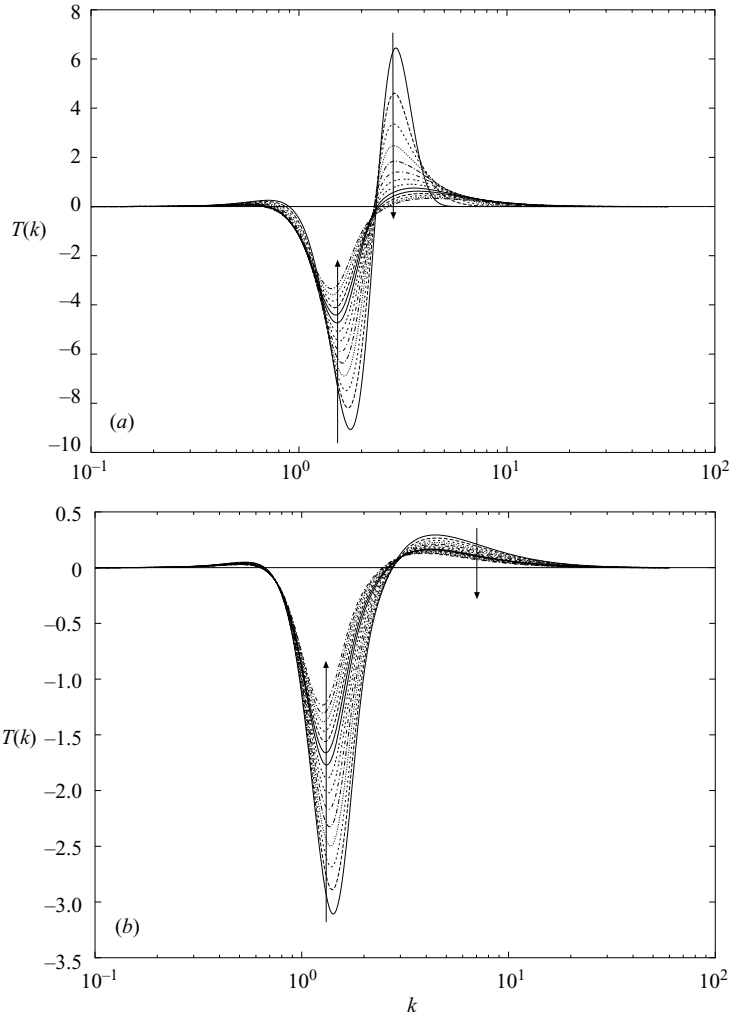

FIGURE 10. Time evolution of the spherically integrated energy transfer spectrum at $Re = 5$, $k_{max} = 60$, $dt = 5 \times 10^{-5}$ between (*a*) $t_0 = 0$ and $t = 0.525$; (*b*) $t = 0.525$ and $t = 1.05$ in steps of 0.0375. Arrows indicate increasing time.

5.2. *Time evolution of total kinetic energy and of single-point indicators of anisotropy*

The modification of the spectral distribution of energy density in rotating turbulence is an indicator of the structuring of the flow, and of its modified dynamics with respect to isotropic turbulence. Upon integration of the energy density spectrum over the complete spectral space, one obtains the total energy $E_t = q^2/2$ in the flow, whose decay is plotted on figure 12(*a*). The power obtained at the end of our computation is -0.8, which shows a strong reduction of energy transfer and hence of the decay rate of turbulence with respect to the isotropic law $t^{-10/7}$. This was again observed by CMG and Squires *et al.* (1994). Comparing with the result obtained from the EDQNM$_2$ model run in the same conditions, we observe on figure 12(*b*) that the decay rate of both models is very similar, since the EDQNM$_2$ model yields a $t^{-0.86}$ power law.

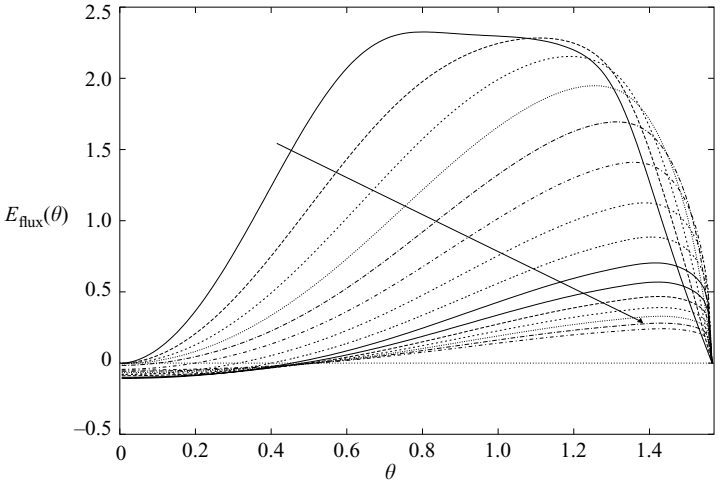

FIGURE 11. Time evolution of the angular flux of energy $E_{\text{flux}}(\theta)$ as a function of θ, at $Re = 5$, $k_{\max} = 60$, $\mathrm{d}t = 5 \times 10^{-5}$, between $t = 0$ and $t = 1.05$.

The large-time, inviscid self-similarity identified earlier can be expressed more precisely by

$$\frac{e(k_s(t)\kappa, \theta, t)}{e_s(t)} \to f(\kappa, \theta), \tag{5.3}$$

at infinite Reynolds number as $t \to \infty$, for any fixed values of the scaled wavenumber $\kappa = k/k_s$ and $\theta \neq \pi/2$, where $k_s(t)$, $e_s(t)$ are appropriate scales for wavenumber and energy density. If such limiting behaviour is assumed for e and the resulting expression,

$$e(\boldsymbol{k}, t) = e_s(t) f(\boldsymbol{k}/k_s(t)), \tag{5.4}$$

is used in the AQNM equation (4.1) (without the viscous term), the wavenumber and energy-density scales can be shown to evolve according to the power laws

$$e_s(t) \propto (t + t_0)^{5\alpha - 1}, \tag{5.5}$$

$$k_s(t) \propto (t + t_0)^{-\alpha}. \tag{5.6}$$

As a result, the total energy, given by the spectral-space volume integral of e, behaves like $(t + t_0)^{2\alpha - 1}$. Figure 12, discussed above, shows that there is indeed a power law, a result which supports the conclusion of self-similarity and whose exponent of -0.8 for the total energy implies $\alpha = 0.1$. Note that such a link between inviscid self-similarity and temporal power laws is a classical one for non-rotating, isotropic turbulence (see e.g. Monin & Yaglom 1975, section 16.1) and that, without self-similarity, a power law is hard to explain. Note also that the scaled, limiting spectrum $f(\kappa, \theta)$ appears to have an integrable singularity at $\theta = \pi/2$.

The full Reynolds stress tensor involves both a spherical and a deviatoric part as $\langle u_i u_j \rangle = q^2(\delta_{ij}/3 + b_{ij})$, the latter deviatoric tensor b_{ij} reflecting anisotropy. Because of the symmetry – axisymmetry without mirror symmetry – the deviatoric tensor can be expressed by only one component, say b_{33}, as $b_{ij} = (-3b_{33}/2)\left(\delta_{ij}/3 - \delta_{i3}\delta_{j3}\right)$. In agreement with the relationship (B 3) in Appendix B, b_{ij} is in general the sum of two different contributions b^e_{ij} and b^z_{ij}, which reflect the directional and the polarization

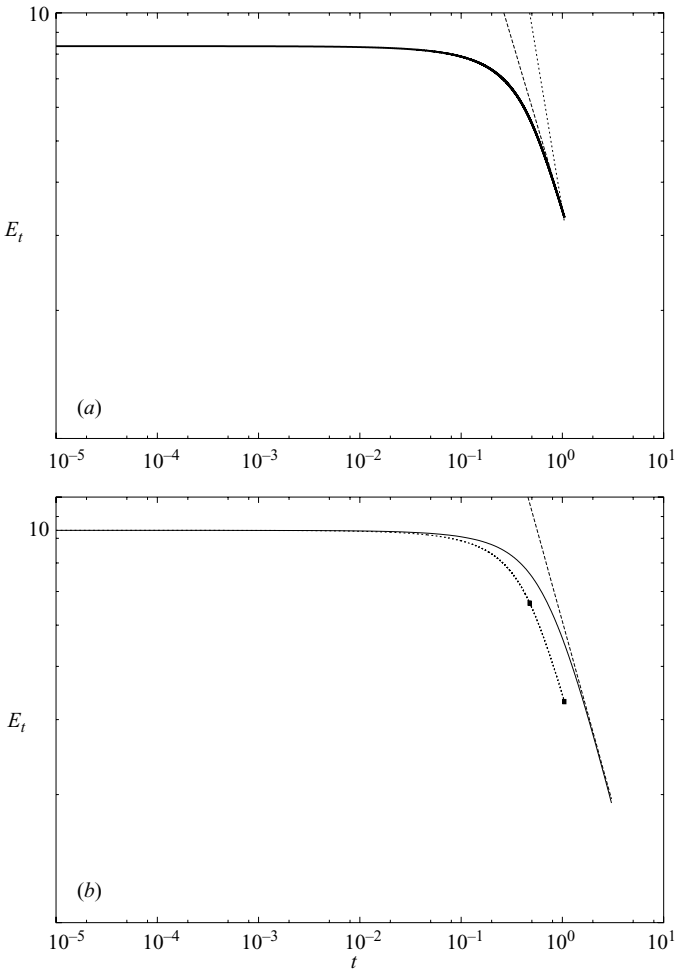

FIGURE 12. (*a*) ———, Time evolution between $t=0$ and $t=1.05$ with $Re=5$, $k_{\max}=60$ and $\mathrm{d}t=5\times10^{-5}$ of the total energy E_t. - - - -, $t^{-0.8}$ and . . . , $t^{-10/7}$ power laws. (*b*) ———, EDQNM_2 and $\cdots$, AQNM decay of total energy E_t. The straight line is a $t^{-0.86}$ law. The black squares show the energy at times $t=0.525$ and $t=1.05$, at which the angular-dependent spectra are plotted on figure 6.

anisotropy respectively. This decomposition here reduces to

$$q^2 b_{33} = \int \left[\left(e - \frac{E}{4\pi k^2} \right) \sin^2\theta + Re(Z\mathrm{e}^{-2\mathrm{i}\sigma t}) \sin^2\theta \right] \mathrm{d}^3\boldsymbol{k} \tag{5.7}$$

with $b_{ij}=b^e_{ij}$ in the absence of a Z-contribution. As shown in figure 13, b^e_{33} starts from zero (three-dimensional isotropy) and saturates at a value close to 0.07–0.08. This value is about half that expected for a pure two-dimensional flow, or $b^e_{33}=1/6$, and recovered in (5.7) using for e a Dirac function $e=(E(k,t)/2\pi k)\delta(k_\parallel)$ (details in CMG, §4). Such a saturated value is also obtained in recent DNS/LES of rotating flows (Morinishi, Nakabayashi & Ren 2001*a*, *b*; Yang & Domaradzki 2004) in which b^e_{ij} is plotted, following CMG (their figure 7). In some DNS/LES results, however, this growth of b^e_{33} is counterbalanced by a stronger decrease of b^z_{33}, resulting in a negative value of b_{33}. This will be discussed in the next section.

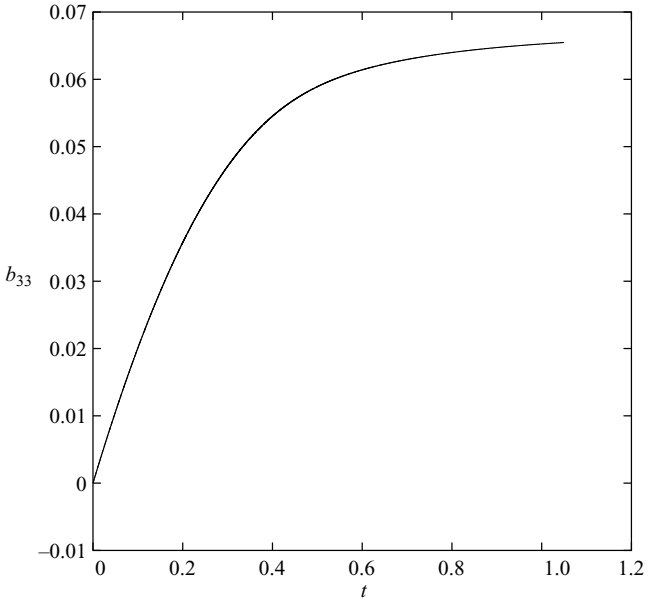

FIGURE 13. Time evolution of the deviatoric component of the Reynolds stress tensor b_{33} at $Re = 5$, $k_{\max} = 60$, $\mathrm{d}t = 5 \times 10^{-5}$, between $t = 0$ and $t = 1.05$.

6. General discussion

Turbulence in a rotating frame illustrates the subtle interplay between linear and nonlinear processes and the significance of spectral anisotropy, especially the angular dependence of spectral energy which reflects dimensionality.

The breaking of isotropy is potentially present in the linear operator since the dispersion law of inertial waves depends on their angle of propagation, as does the anisotropic definition of the helical modes. Nevertheless, this potential anisotropy is not necessarily reflected in statistical quantities. The second-order spectral tensor – single-time two-point velocity correlations – remains isotropic in the linear regime, as shown by the system of equations (2.19)–(2.21) with zero right-hand sides. A possible breaking of isotropy through two-time velocity correlations is not discussed here for the sake of brevity (see Cambon *et al.* 2004*a*). Going back to equation (2.19), it is clear that isotropy is broken in the energy equation by the energy transfer term through single-time triple correlations. Isotropy breaking in our case comes first from the linear operators which act on triple velocity correlations as a product of three Green's functions (e.g. equation (2.25)).

6.1. *Directional anisotropy*

In addition to the detailed dependence of the energy spectra on the wavenumber k and the angle θ, the AQNM model yields a k^{-3} scaling for the inertial spectral subrange. This law is very different from the one found in two-dimensional turbulence, which corresponds to $E^{2D}(k_\perp) \sim \overline{\omega^2} k_\perp^{-3}$ with enstrophy ($\overline{\omega^2}$) conservation. Our $E(k)$ is three-dimensional and would reduce to the former only if $e = (E(k)/2\pi k)\delta(k_\parallel)$. Even though some authors advocated two-dimensionalization of turbulence by rapid rotation from forced under-resolved DNS (e.g. Hossain 1994), and tried to interpret a k^{-3} law along this line, our results are not consistent with two-dimensionalization. Looking at the explicit θ-dependent spectra, we propose that, since the horizontal wavevectors exhibit a decay exponent larger than -3 with k whereas oblique ones

decay with a smaller exponent, a combination of these is necessary to achieve the k^{-3} behaviour.

We note that the full (k, θ) distribution of the energy-density spectrum obtained with AQNM is very much like that obtained in previous works with the EDQNM model and LES of rotating homogeneous turbulence. The spectral anisotropy is reflected in a specific anisotropic structuring of the flow when using specifically weighted integrals of the energy spectrum.

The reader is referred to Galtier (2003) and CRG for a discussion of analytical laws obtained from WT with additional assumptions ($k_\parallel \ll k_\perp$) compared with our AQNM numerical results. Galtier's proposal $e \sim k_\parallel^{-1/2} k_\perp^{-7/2}$ is consistent with the k^{-2} law for $k^2 e(k, \theta, t)$ at the smallest $\cos\theta = k_\parallel / k$ (figure 6), but a significant inverse cascade is found by AQNM in this domain, which is not allowed by Galtier's analysis. On figure 9(*a*), the curve representing $(\cos\theta)^{-1/2}$ suggested by Galtier's analysis is plotted against the AQNM results.

6.2. *Relevance of AQNM and the role of the quasi-slow manifold*

As discussed earlier, the asymptotics leading to (4.1) suffer from non-uniformity for $\boldsymbol{k}$ near the horizontal plane. This comes about because (2.22) with (3.1) consists of oscillatory exponential terms of frequency $(s_3 + s_4 - s - s')\sigma_k$. For $\boldsymbol{k}$ which are not close to the horizontal plane, these exponentials are rapidly oscillatory, and hence dropped in the asymptotic analysis, unless $s_3 + s_4 = s + s'$. However, if $\boldsymbol{k}$ is close to horizontal, σ_k is small and the terms are no longer rapidly oscillating. As a result, there is a small region of angles near $\theta = \pi/2$ in which a more complete asymptotic description should be used.

Despite the above non-uniformity, the model provides a self-consistent description of wavevectors away from the horizontal plane, because it predicts only an integrable singularity in the energy density. Whether or not the near-horizontal region is important depends on which statistical quantity is required. For instance, the spherically averaged spectrum and total energy will be negligibly affected, whereas other quantities depend on the details of near-horizontal wavenumber spectra, for example, the integral length scales with vertical separation defined by (Cambon & Jacquin 1989)

$$\overline{u_1^2} L_{11}^{(3)} = \overline{u_2^2} L_{22}^{(3)} = \pi^2 \int_0^\infty (e(k, \cos\theta = 0) - Z(k, \cos\theta = 0))\, k \, \mathrm{d}k,$$

$$\overline{u_3^2} L_{33}^{(3)} = 2\pi^2 \int_0^\infty (e(k, \cos\theta = 0) + Z(k, \cos\theta = 0))\, k \, \mathrm{d}k.$$

AQNM is capable of predicting any statistical quantity of the first kind; the current results for the spherically averaged energy spectrum and in § 5.2 for the Reynolds stress tensor are unlikely to be modified by the refined analysis of the slow manifold. An important feature of the extended WT theory is the emergence of the polarization anisotropy Z, which is therefore zero almost everywhere but in the slow manifold, as well as in our case where AQNM is started with three-dimensional isotropy. It can therefore be inferred that the contribution of Z is unimportant for deriving e.g. the Reynolds stress tensor, but is essential if the behaviour of typical integral length scales is concerned.

A possible means of treating the near-horizontal wavevectors is discussed in CRG with a proposal for using matched expansions with a specific inner model for the slow manifold, and AQNM as the outer model. The way to perform this analysis is

suggested by the general $EDQNM_{2-3}$ model (detailed $EDQNM_3$ equations are given in CRG, appendix) which underlies the AQNM model.

A nonlinear Proudman theorem is often invoked, which means the independence of the slow manifold, which could be governed by its own equations in accordance with autonomous two-dimensional dynamics. This argument is supported by mathematical developments for some classes of initial data (Babin *et al.* 1999), and not by others (Babin *et al.* 2001). It is important to point out that periodicity conditions are used, and that the possible decoupling of the two-dimensional manifold from the rest is only valid at the first order. Our AQNM approach is essentially different since our equations (and those of Galtier 2003) were found in a continuous unbounded domain, excluding the exact two-dimensional manifold. This 'nonlinear Proudman theorem' is either irrelevant, if the slow mode is unimportant because of its integrable singularity, or questionable at largest times, if the slow mode is analysed by itself and/or for specific quantities which rely only upon it. In this second case, the analysis introduced by CRG, even if not analytically developed, demonstrates a typical coupling between the slow and rapid modes through new volume and principal value integrals, with respect to AQNM. These coupling terms are neglected in AQNM when discarding those terms considered as rapidly oscillating.

6.3. *Two-dimensional or not two-dimensional?*

As we have seen, our results indicate the transfer of energy towards horizontal wavevectors and also the appearance of large energy densities near the horizontal plane. At first glance, this suggests the possibility that the flow becomes two-dimensional. However, this is not the case for the following reasons. First, following the development phase and hence at large times, the spectrum evolves in a self-similar manner (recall figures 6 and 7). This outcome excludes two-dimensionalization in the limit of large time. Secondly, as indicated by figure 9, the overall energy is not dominated by horizontal wavevectors as it would be for a two-dimensional flow. Figure 9 also illustrates the singularity in the energy density.

DNS and LES results have also shown the tendency of rotating turbulence to become anisotropic by transfer towards the horizontal plane. For instance, Bartello, Métais & Lesieur (1994) showed the development of vortices elongated in the vertical direction, while CMG determined the time evolution of spectra leading to results comparable with those of figure 5. However, it is difficult to decide, based on these results, whether the flow becomes two-dimensional in the large-time limit, for several reasons. Spatial periodicity of the flow, which is assumed numerically, implies that the size of the periodic box must be sufficiently large in order to avoid effects of numerical confinement. In particular, the turbulent correlation length should be small compared with the box size, as should $c_g t$ where c_g is the group velocity associated with inertial waves. The latter condition becomes harder to satisfy the longer the time simulated. Since the evolution time at small Rossby number scales as $Ro^{-2}\Omega^{-1}$, the limit of small Ro is particularly hard to treat.

6.3.1. *Reynolds stress tensor anisotropy*

Regarding Reynolds stress tensor (RST) anisotropy with directional/polarization splitting, recent DNS/LES (CMG; Morinishi *et al.* 2001*a*; Yang & Domaradzki 2004) with correct resolution show results similar to those of AQNM for the b^e_{33} history, also in agreement with $EDQNM_2$ (CMG). The maximum value eventually reached is never larger than 0.08, i.e. very close to the AQNM limit, and therefore remained far from the theoretical two-dimensional limit which is 1/6. In addition, a rapid evolution

of b_{33}^z can yield a strong departure of b_{33} from b_{33}^e, resulting eventually in a negative value of b_{33} (Yang & Domaradzki 2004). Even though a significant value of Z is expected in the slow manifold (see CMG and CRG), in agreement with the behaviour of the integral length scales with vertical separation, we find it highly questionable that this term could contribute dominantly to the RST anisotropy. Hence, the significant negative value of b_{33}^z which contaminates b_{33} is probably due to the following causes:

(*a*) isotropy is not precisely controlled in the initial data, and strong departures from axisymmetry appear ($b_{11} \neq b_{22}$) only after small elapsed times (Yang & Domaradzki 2004);

(*b*) the numerical box is too small given the huge elapsed time used, so that an artificial confinement biases the most elongated scales;

(*c*) the angular-phase mixing in (5.7), due to the term $\mathrm{e}^{-2\mathrm{i}\sigma t}$, which can damp any Z contribution is not accurately computed in DNS.

Drawbacks (*a*, *b*) were not present in the LES database in CMG, with an aspect ratio of 4 (resolution $512 \times 128 \times 128$) optimized to control the anisotropy (initial isotropy becoming axisymmetry) and to avoid artificial confinement. Nevertheless, a second transition occurred, with b_{33}^z becoming significantly negative, although b_{33} itself never became negative. This result has to be considered with care, since the typical Rossby number based on the cutoff wavenumber became of the order of unity and unexpected oscillations appeared after the second transition. Note that in their 64^3 DNS/LES, Bartello *et al.* (1994) found strong negative values of b_{33}, without using the b_{ij}^e, b_{33}^z splitting. As a final comment, it is important to point out that a positive value of b_{33} in true axisymmetrical turbulence means $a = \langle u_\parallel^2 \rangle / \langle u_\perp^2 \rangle$ larger than one ($a = 2$ if $b_{33} = 1/6$) whereas a negative value of b_{33} means a smaller than one ($a = 0$ if $b_{33} = -1/3$). This illustrates that dimensionality and polarization may have opposite effects on the RST anisotropy, or componentality (see also Reynolds & Kassinos 1995). In this view, DNS/LES may exhibit a two-component limit instead of a two-dimensional one, due to low resolution, but also because the ensemble averages needed to obtain reliable statistics are not available from one realization only.

6.3.2. k^{-3} *slope*

From the sole fact that the energy transfer scales as $1/\Omega$, a k^{-2} slope could be inferred for the spherically averaged energy spectrum (Zhou 1995), but this oversimplified argument ignores anisotropy. In contrast, our results indicate k^{-3} for the spherically averaged spectrum in the inertial range. According to the power laws, (5.5) and (5.6), arising from self-similarity of the three-dimensional spectrum, the spherically averaged spectrum should behave as $t^{3\alpha-1}$ at large time. Given k^{-3} behaviour, this leads to an inertial-range spectrum like $t^{-1}k^{-3}$, with a purely numerical prefactor. This result, when expressed in dimensional terms, implies that the inertial-range spherically averaged spectrum scales as $\Omega t^{-1} k^{-3}$, independent of the initial spectral parameters. Comparison of the spectra in figure 4(*b*) at $k = 2$ and the two times $t = 0.525$ and $t = 1.05$ shows a decrease by a factor of very nearly 2 (to within a few percent). Such close correspondence with the t^{-1} law provides further confirmation of the hypothesis of self-similarity.

From a review of DNS/LES of decaying turbulence, it seems that only Yang & Domaradzki (2004) found a clear transition from k^{-2} to k^{-3}, the latter result being in qualitative agreement with our AQNM results. Forced DNS/LES often suffer from numerical biases even worse than those in the free decay, so that only the study by Smith & Waleffe (1999) (SW) is discussed here, in which the forcing is truly isotropic and limited to a small-scale region with wavenumber k_f. Before

comparing their results with our AQNM (numerical) ones, it is important to stress some different definitions of spectra. In order to avoid ambiguity, the spherically averaged spectrum and its counterpart near the 'slow manifold' in SW will be referred to as $E^N(k)$ and $E^N(k_\parallel, k_\perp)$. It now appears that $E^N(k)$ is the same as our $E(k)$, but a prefactor $k_\perp$ has to be introduced to compare the second spectrum with our e, so that $e(k, \cos\theta) \sim k_\perp E^N(k_\parallel, k_\perp)$. Accordingly, the result of SW for the slow manifold, for k smaller than k_f, or $E^N(k_\perp, k_\parallel) \sim k_\perp^{-3}$, is consistent with the law $k^2 e(k, \cos\theta \sim 0) \sim k^{-2}$ shown in figure 6 for the smallest values of $\cos\theta = k_\parallel/k = k_\parallel/\sqrt{k_\parallel^2 + k_\perp^2}$, since $k \sim k_\perp$ in the spectral domain considered. On the other hand, the collapse of $E^N(k)$ and $E^N(k_\parallel = 0, k_\perp)$ observed in SW at the smallest k, interpreted as a sign of two-dimensionalization of the largest scales, is not obtained in our AQNM results, so that the similar k^{-3} laws obtained for both E^N (SW) and E (AQNM) probably have different causes. The results of SW have two consequences: an energy transfer from small to large scales was shown, although different from the classical pure two-dimensional dynamics one; strong coupling between rapid and slow modes is shown, with no independence of the slow manifold. The scaling $E^N(k_\parallel = 0, k_\perp) \sim k_\perp^3$ is confirmed by Smith & Lee (2005), restricting the calculation to near-resonant triads.

7. Conclusion

In this work, we propose a nonlinear model for the dynamics of inertial waves in the limit of high Reynolds number and low Rossby number. We show that the asymptotic behaviour of turbulence can be described independently of the explicit value of the rotation rate, viscosity remaining only as a means of regularizing the equations at the large-wavenumber numerical cutoff. The derivation of the asymptotic quasi-normal model is started from the existing anisotropic eddy-damped quasi-normal statistical model, which includes part of the Green's function influence on second- and third-order velocity correlations, coming from inertial waves. Instead of integrating the energy transfer over all possible interaction triads of inertial waves, the AQNM model is simplified compared to the EDQNM one by reducing the integration over resonant triads of inertial waves, which are shown to emerge in the limit of fast rotation. Thus, asymptotic analysis leads to a Lin-type energy equation, with energy transfer computed over surfaces of resonant interactions only. Handling the complex topology of these surfaces is the price to pay for the simplification of the integral. The most important and original part of this work is that we propose a numerical implementation of the AQNM model, and obtain quantitative results for the evolution of the energy-density spectrum, to be contrasted with the qualitative results obtained in previous wave turbulence studies through assumptions of a specific scaling of the spectra.

The model predicts a development phase in which both anisotropy and an inertial range appear. Subsequently, spectral power laws are found in which the spherically averaged inertial range spectrum behaves like k^{-3}. However, this represents the average of power laws whose exponents depend on the wavevector direction: the exponent runs from -2 to -4, depending on the angle considered. The spectral evolution is observed to be self-similar at large times, an outcome which excludes two-dimensionalization of the flow in the limit $t \to \infty$. The energy density is found to be large for nearly horizontal wavevectors, apparently reflecting a singularity at the horizontal plane. However, this singularity is integrable, and so quantities like the spherically averaged spectrum and Reynolds stresses are not dominated by this

singularity. This may be contrasted with the two-dimensional case in which the horizontal plane contains all the energy. Finally, the kinetic energy decays as $t^{-0.8}$.

The numerical part of the work was possible thanks to parallel computing time offered by the following national computing centers: Centre Informatique National de l'Enseignement Suprieur (CINES, Montpellier); Commissariat à l'énergie Atomique (CEA-CENG, Grenoble); Institut du Développement et des Ressources en Informatique Scientifique (IDRIS, Orsay).

Appendix A. Poloidal–toroidal decomposition, and Craya–Herring frame of reference

The poloidal–toroidal decomposition is used to represent a three-component divergence-free velocity field in terms of two independent scalar terms, taking advantage of the presence of a privileged direction $\boldsymbol{n}$:

$$\boldsymbol{u} = \nabla \times (s_{pol}\boldsymbol{n}) + \nabla \times [\nabla s_{tor} \times \boldsymbol{n}] \tag{A 1}$$

the axial vector $\boldsymbol{n}$ being chosen along the vertical direction, without loss of generality. As a caveat, some care is needed to represent a vertically sheared horizontal flow (VSHF, after Smith & Waleffe (2002) or $\boldsymbol{u}(\boldsymbol{x}\cdot\boldsymbol{n}, t)$, with $\boldsymbol{u}\cdot\boldsymbol{n} = 0$, with this decomposition.

In Fourier space, the above decomposition yields a pure geometrical one, or

$$\hat{u} = \boldsymbol{k} \times \boldsymbol{n}(\mathrm{i}\hat{s}_{pol}) - \boldsymbol{k} \times (\boldsymbol{k} \times \boldsymbol{n})(\hat{s}_{tor}) \tag{A 2}$$

and it appears immediately that the Fourier mode related to the vertical wavevector direction, or $\boldsymbol{k} \parallel \boldsymbol{n}$, has zero contribution; this 'hole' in the spectral description yields the missing VSHF mode in physical space. In order to complete the decomposition, one can define an orthonormal frame of reference, which is in fact the local reference frame of a polar spherical system of coordinates for $\boldsymbol{k}$:

$$\boldsymbol{e}^{(1)} = \frac{\boldsymbol{k} \times \boldsymbol{n}}{|\boldsymbol{k} \times \boldsymbol{n}|}, \quad \boldsymbol{e}^{(2)} = \boldsymbol{e}^{(3)} \times \boldsymbol{e}^{(1)}, \quad \boldsymbol{e}^{(3)} = \frac{\boldsymbol{k}}{k}, \tag{A 3}$$

for $\boldsymbol{k} \times \boldsymbol{n} \neq 0$, and $\boldsymbol{e}^{(1)}, \boldsymbol{e}^{(2)}, \boldsymbol{e}^{(3)}$ may coincide with the fixed frame of reference, with $\boldsymbol{e}^{(3)} = \boldsymbol{n}$ for $\boldsymbol{k} \parallel \boldsymbol{n}$. In the turbulence community, the local frame $(\boldsymbol{e}^{(1)}, \boldsymbol{e}^{(2)})$ of the plane normal to the wavevector is often referred to as the Craya–Herring frame. Accordingly, the divergence-free velocity field in wave-space has only two components in the Craya–Herring frame, or

$$\hat{\boldsymbol{u}}(\boldsymbol{k}, t) = u^{(1)}\boldsymbol{e}^{(1)} + u^{(2)}\boldsymbol{e}^{(2)}. \tag{A 4}$$

For $\boldsymbol{k} \times \boldsymbol{n} \neq 0$, $u^{(1)}$ and $u^{(2)}$ are directly linked to the toroidal mode and the poloidal mode, respectively. For $\boldsymbol{k} \times \boldsymbol{n} = 0$, they correspond to the VSHF mode. RDT equations can be written in the Craya–Herring frame, resulting in a reduced Green's function with only four independent components (Cambon 1982). A similar decomposition is used in Bartello *et al.* (1994). Finally, the 'wave-vortex' decomposition introduced by Riley, Metcalfe & Weissman (1981) in the particular context of stably stratified turbulence, is also a particular case of (A 1).

Appendix B. Anisotropic description for second-order statistics

Independently of closure, the spectral tensor Φ_{ij} is not a general complex matrix, but has a number of special properties, including the fact that it is Hermitian,

positive-definite, and satisfies $\Phi_{ij}k_j = 0$, obtained from the incompressibility condition $k_j\widehat{u}_j = 0$. Taken together, these properties mean that, instead of the 18 real degrees of freedom of a general complex tensor, Φ_{ij} has only four. Indeed, using a spherical polar coordinate system in $\boldsymbol{k}$-space, or (A 3) and (A 4), the tensor takes the form

$$\boldsymbol{\Phi} = \begin{pmatrix} e-\zeta_r & -\zeta_i + \mathrm{i}h & 0 \\ -\zeta_i - \mathrm{i}h & e+\zeta_r & 0 \\ 0 & 0 & 0 \end{pmatrix} \tag{B 1}$$

see CMG for details, in which ζ^* was denoted Z). The scalars $e(\boldsymbol{k}, t)$ and $h(\boldsymbol{k}, t)$ are real, and $\zeta(\boldsymbol{k}, t) = \zeta_r + \mathrm{i}\zeta_i$ is complex. The spectrum $e(\boldsymbol{k}, t) = \frac{1}{2}\Phi_{ii}$ is the energy density in $\boldsymbol{k}$-space, whereas $h(\boldsymbol{k}, t) = (-1/2)\mathrm{i}k_l\epsilon_{lij}\Phi_{ij}/k$ is the helicity spectrum and, along with ζ, is zero in the isotropic case.

Anisotropy is expressed through variation of these scalars with the direction of $\boldsymbol{k}$, as well as departures of h and ζ from zero at a given wavenumber. Whatever spectral closure is used, the number of real unknowns may be reduced to the above four when carrying out numerical calculations, and the presentation of the results can be simplified using these variables, particularly when the flow is axisymmetric.

In tensorial form, the contributions from e, ζ, h in (B 1) are rewritten as

$$\Phi_{ij} = e(\boldsymbol{k}, t)P_{ij}(\boldsymbol{k}) + \mathrm{Re}[\zeta^*(\boldsymbol{k}, t)N_i(\boldsymbol{k})N_j(\boldsymbol{k})] + \mathrm{i}h(\boldsymbol{k}, t)\epsilon_{ijn}\frac{k_n}{k} \tag{B 2}$$

in which $P_{ij} = \delta_{ij} - k_ik_j/k^2$ is the projector and $\boldsymbol{N} = \boldsymbol{e}^{(2)} - \mathrm{i}\boldsymbol{e}^{(1)}$ using (A 3). The anisotropic contributions are separated from the isotropic one in (B 2) as

$$\mathrm{Re}\left(\Phi_{ij}\right) = \underbrace{\frac{E(k)}{4\pi k^2}P_{ij}}_{\text{isotropic}} + \underbrace{\left(e(\boldsymbol{k}) - \frac{E(k)}{4\pi k^2}\right)P_{ij}}_{\text{directional anisotropy}} + \underbrace{\mathrm{Re}\left(\zeta^*(\boldsymbol{k}, t)N_iN_j\right)}_{\text{polarization anisotropy}} \tag{B 3}$$

with a subsequent splitting of any second-order statistical quantity.

Appendix C. Integration in the vicinity of resonant surfaces

In the limit $d = \mu_{kpq} \to 0$, the integrand of (3.3) – likewise for (3.4) – comprises a regular and a singular contribution which can be transformed into surface integrals with some additional assumptions.

Considering a resonant surface given by the couple (s', s''), the integral is mainly contributed to by wavevectors $\boldsymbol{k}$ which are close to the resonant surface, since the integrand behaves as a Dirac function. One can therefore neglect the far wavevectors contribution, and focus on a small volume V_ε around the resonant surface $F_{s's''} = 0$, with thickness 2ε. Figure 14 is a sketch of a piece of the resonant surface, and of the local system of coordinates. We introduce the local curvilinear coordinates (q_1, q_2) over the resonant surface, and complete them with a third coordinate ξ, which represents the distance between a point in space close to the surface to the closest one on the resonant surface. Positive values of ξ are along increasing F, and ξ is zero at the surface. Each wavevector is associated with a point in space, so that $\boldsymbol{p}$ spans the volume around the resonant surface, and $\boldsymbol{k}'$ is the vector associated with the closest point on the surface, consistently with the definition of ξ.

In the integrals (3.3) and (3.4), the non-singular terms $g_{s's''}(\boldsymbol{p})$ and $A_{s's''}(\boldsymbol{p})$ are slowly varying functions in the neighbourhood of the resonant surface, with respect to the variations of d. They are therefore equated to their values at $\boldsymbol{k}'$. On the other

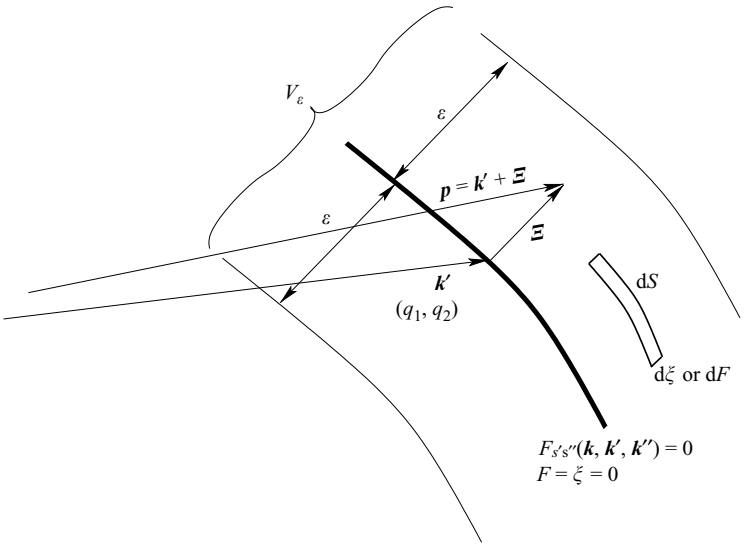

FIGURE 14. General curvilinear coordinate system in the neighbourhood of a resonant surface.

hand, $F_{s's''}$ is expanded in the direction orthogonal to the resonant surface, in order to remove the singularity. The first-order Taylor expansion around $\boldsymbol{k}'$ is

$$F(\boldsymbol{p}) = F(\boldsymbol{k}' + \boldsymbol{\Xi}) = F(\boldsymbol{k}') + \boldsymbol{\Xi} \cdot \nabla F(\boldsymbol{k}'). \tag{C 1}$$

Higher-order terms correspond to higher-order resonance, and are neglected. Since $F(\boldsymbol{k}') = 0$ and the gradient of F is parallel to $\boldsymbol{\Xi}$, $\boldsymbol{\Xi} \cdot \nabla F(\boldsymbol{k}') = \xi \left|\nabla F(\boldsymbol{k}')\right|$ and (C 1) becomes $F(\boldsymbol{p}) = \xi |\nabla F(\boldsymbol{k}')|$. Using the inertial wave group velocity $\boldsymbol{C}$, another expression for the gradient is $\nabla F(\boldsymbol{k}') = s'\boldsymbol{C}(\boldsymbol{k}') - s''\boldsymbol{C}(-\boldsymbol{k} - \boldsymbol{k}')$, and yields $|\nabla F(\boldsymbol{k}')| = \pi \alpha_{s's''}(\boldsymbol{k}', -\boldsymbol{k} - \boldsymbol{k}')$, with $\alpha_{s's''}(\boldsymbol{k}', \boldsymbol{k}'') = |s'\boldsymbol{C}(\boldsymbol{k}') - s''\boldsymbol{C}(\boldsymbol{k}'')|/\pi$. Finally, we obtain

$$F(\boldsymbol{p}) = \pi \alpha_{s's''}(\boldsymbol{k}', -\boldsymbol{k} - \boldsymbol{k}')\xi,$$

which is introduced in the volume integrals with the $(\mathrm{d}\xi, \mathrm{d}q_1, \mathrm{d}q_2)$ parameterization of the volume element. For (3.3) written in the coordinates (q_1, q_2, ξ) with the element of surface dS from dq_1 and dq_2 this yields

$$\int_{\mathbb{R}^3} g(\boldsymbol{p}) \frac{d}{d^2 + F(\boldsymbol{p})^2} A_{ss'}(\boldsymbol{p}, t)\, \mathrm{d}^3\boldsymbol{p} = \iint \left[\int \frac{d}{d^2 + \pi^2 \alpha_{s's''}{}^2(\boldsymbol{k}', -\boldsymbol{k} - \boldsymbol{k}')\xi^2} \mathrm{d}\xi \right] g(\boldsymbol{k}') A_{ss'}(\boldsymbol{k}', t)\, \mathrm{d}S,$$

where the ξ integration is performed through the resonant surface. The corresponding integrand goes to zero as ξ^{-2} when $\xi \to \infty$, so that the integration is extended from $-\infty$ to ∞ rather than a neighbourhood of the resonant surface, and can be performed analytically:

$$\int_{-\infty}^{+\infty} \frac{d}{d^2 + \pi^2 \alpha^2 \xi^2} \mathrm{d}\xi = \frac{1}{\alpha}.$$

We thus finally obtain surface integrals as the asymptotic approximations for the coefficients

$$B_s(\boldsymbol{k},t) = -2\sum_{s',s''}\int_{S_{s's''}} \frac{g_{s's''}}{\alpha_{s's''}} A_{ss'}(\boldsymbol{k}',t)\,\mathrm{d}S \tag{C 2a}$$

$$= -2\pi\sum_{s',s''}\int_{\mathbb{R}^3} \delta(F_{s's''}) g_{s's''} A_{ss'}(\boldsymbol{p},t)\,\mathrm{d}^3\boldsymbol{p}, \tag{C 2b}$$

$$C_s(\boldsymbol{k},t) = 2\sum_{s's''}\int_{S_{s's''}} \frac{\gamma_{s's''}}{\alpha_{s's''}} A_{ss'}(\boldsymbol{k}',t) A_{ss''}(\boldsymbol{k}'',t)\,\mathrm{d}S \tag{C 3a}$$

$$= 2\pi\sum_{s's''}\int_{\mathbb{R}^3} \delta(F_{s's''}) \gamma_{s's''} A_{ss'}(\boldsymbol{p},t) A_{ss''}(\boldsymbol{q},t)\,\mathrm{d}^3\boldsymbol{p}, \tag{C 3b}$$

where $S_{s's''}$ is the resonant surface for the choice of parameters $(\boldsymbol{k}, s', s'')$ (see equation (3.6)). Expressions (C 2*b*) and (C 3*b*) come from (3.3) and (3.4) in which the functions involving μ_{kpq} have been replaced by Dirac functions of the resonant surface, multiplied by π. Regarding $D(\boldsymbol{k},t)$, the same procedure is applied to its real part so that

$$D(\boldsymbol{k},t) = -\sum_{s',s''}\int_{S_{s's''}} \frac{g_{s's''}}{\alpha_{s's''}} e(\boldsymbol{k}',t)\,\mathrm{d}S - \mathrm{i}\sum_{s',s''}\int_{\mathbb{R}^3} g_{s's''}\frac{F_{s's''}}{d^2+{F_{s's''}}^2} e(\boldsymbol{p},t)\,\mathrm{d}^3\boldsymbol{p}.$$

The imaginary part has to be treated differently, since the singularity cannot be removed by merely letting d go to zero. One has to examine the separate contributions of domains far from the resonant surface, and in its neighbourhood V_ε:

$$\mathrm{Im}[D(\boldsymbol{k},t)] = -\sum_{s',s''}\int_{\mathbb{R}^3\setminus V_\varepsilon} g_{s's''}\frac{F_{s's''}}{d^2+{F_{s's''}}^2} e(\boldsymbol{p},t)\,\mathrm{d}^3\boldsymbol{p} - \sum_{s',s''}\int_{V_\varepsilon} g_{s's''}\frac{F_{s's''}}{d^2+{F_{s's''}}^2} e(\boldsymbol{p},t)\,\mathrm{d}^3\boldsymbol{p}. \tag{C 4}$$

Away from the resonant surface, i.e. removing V_ε from the integration domain, given ε, the asymptotic limit yields

$$\lim_{d\to 0}\left[-\sum_{s',s''}\int_{\mathbb{R}^3\setminus V_\varepsilon} g_{s's''}\frac{F_{s's''}}{d^2+{F_{s's''}}^2} e(\boldsymbol{p},t)\,\mathrm{d}^3\boldsymbol{p}\right] = -\sum_{s',s''}\int_{\mathbb{R}^3\setminus V_\varepsilon}\frac{g_{s's''}}{F_{s's''}} e(\boldsymbol{p},t)\,\mathrm{d}^3\boldsymbol{p}. \tag{C 5}$$

Letting ε go to zero, this integral tends to the principal value integral over the entire domain $\mathbb{R}^3$ denoted as

$$\lim_{\varepsilon\to 0}\left[-\sum_{s',s''}\int_{\mathbb{R}^3\setminus V_\varepsilon}\frac{g_{s's''}}{F_{s's''}} e(\boldsymbol{p},t)\,\mathrm{d}^3\boldsymbol{p}\right] = -\sum_{s',s''}\fint_{\mathbb{R}^3}\frac{g_{s's''}}{F_{s's''}} e(\boldsymbol{p},t)\,\mathrm{d}^3\boldsymbol{p}.$$

We now consider the integral over V_ε in (C 4), when $d\to 0$. In the curvilinear coordinates (q_1, q_2, F) the elementary volume is $\mathrm{d}^3\boldsymbol{p} = J(q_1,q_2,F)\,\mathrm{d}q_1\,\mathrm{d}q_2\,\mathrm{d}F$, where $J(q_1,q_2,F)$ is the Jacobian of the coordinate transformation. We assume that throughout V_ε the functions are smooth enough to admit a Taylor expansion of the form

$$g_{s's''}(q_1,q_2,F) e(q_1,q_2,F) J(q_1,q_2,F) = \sum_{i=0}^{+\infty}\alpha_i(q_1,q_2)F^i,$$

so that the second term of (C 4) becomes

$$\sum_{s',s''}\int\sum_{i=0}^{+\infty}\alpha_i(q_1,q_2)\left[\int_{F_-}^{F_+}\frac{F^{i+1}}{F^2+d^2}\,\mathrm{d}F\right]\mathrm{d}q_1\,\mathrm{d}q_2, \tag{C 6}$$

The limits F_+ and F_- are functions of q_1, q_2 such that $F_+(q_1,q_2)$ and $F_-(q_1,q_2)$ are the values of F respectively at (q_1,q_2,ε) and $(q_1,q_2,-\varepsilon)$ in the local coordinates system (q_1,q_2,ξ).

If $i\geqslant 1$ the fraction in F is non-singular at vanishing d so that for this limit:

$$\int_{F_-}^{F_+}F^{i-1}\,\mathrm{d}F=\left[\frac{F^i}{i}\right]_{F_-}^{F_+}=\frac{{F_+}^i-{F_-}^i}{i}. \tag{C 7}$$

When $i=0$ the integral is computed as

$$\int_{F_-}^{F_+}\frac{F}{F^2+d^2}\,\mathrm{d}F=\frac{1}{2}\left[\log\left|F^2+d^2\right|\right]_{F_-}^{F_+}=\frac{1}{2}\log\left|\frac{{F_+}^2+d^2}{{F_-}^2+d^2}\right|,$$

prior to taking the limit $d\to 0$:

$$\int_{F_-}^{F_+}\frac{F}{F^2+d^2}\,\mathrm{d}F\to\log\left|\frac{F_+}{F_-}\right|.$$

Equation (C 6) then becomes

$$\sum_{s',s''}\int\left[\sum_{i=1}^{+\infty}\alpha_i(q_1,q_2)\frac{{F_+}^i-{F_-}^i}{i}+\alpha_0(q_1,q_2)\log\left|\frac{F_+}{F_-}\right|\right]\mathrm{d}q_1\,\mathrm{d}q_2. \tag{C 8}$$

Since F is zero on the surface, it admits a power series expansion in ξ in the form of $F(q_1,q_2,\xi)=\sum_{i=1}^{+\infty}F^{(i)}(q_1,q_2)\xi^i$, whence $F_-(q_1,q_2)=\sum_{i=1}^{+\infty}F^{(i)}(q_1,q_2)(-\varepsilon)^i$ and $F_+(q_1,q_2)=\sum_{i=1}^{+\infty}F^{(i)}(q_1,q_2)\varepsilon^i$. This is used when taking the limit $\varepsilon\to 0$ to show that F_- and $F_+\to 0$ and $|F_+/F_-|\to 1$, which proves that the integral (C 8) cancels out at the limit.

The asymptotic imaginary part of $D(\boldsymbol{k},t)$ is finally

$$\mathrm{Im}[D(\boldsymbol{k},t)]=-\sum_{s',s''}\!\!\!\!\!\!\int_{\mathbb{R}^3}\frac{g_{s's''}}{F_{s's''}}e(\boldsymbol{p},t)\,\mathrm{d}^3\boldsymbol{p},$$

yielding the asymptotic $D(\boldsymbol{k},t)$ as equation (3.11).

Appendix D. Derivation of the geometrical factor $g_{s's''}$

As proposed by e.g. Cambon (1982), Waleffe (1993) or Turner (1999), an optimal factorisation of geometric coefficients is obtained by substituting into the local frame defined from the helical mode decomposition ($\boldsymbol{N}(s\boldsymbol{k})$, $\boldsymbol{N}(s'\boldsymbol{p})$, $\boldsymbol{N}(s''\boldsymbol{q})$) an alternative one ($\boldsymbol{W}$, $\boldsymbol{W}'$, $\boldsymbol{W}''$) having its polar axis normal to the plane of the triad rather than to the plane of rotation, such that

$$\boldsymbol{N}(s\boldsymbol{k})=\mathrm{e}^{s\mathrm{i}\lambda}\underbrace{(\boldsymbol{\beta}+\mathrm{i}s\boldsymbol{\gamma})}_{\boldsymbol{W}(s)},\quad \boldsymbol{N}(s'\boldsymbol{p})=\mathrm{e}^{s'\mathrm{i}\lambda'}\underbrace{(\boldsymbol{\beta}'+\mathrm{i}s'\boldsymbol{\gamma})}_{\boldsymbol{W}'(s')},\quad \boldsymbol{N}(s''\boldsymbol{q})=\mathrm{e}^{s''\mathrm{i}\lambda''}\underbrace{(\boldsymbol{\beta}''+\mathrm{i}s''\boldsymbol{\gamma})}_{\boldsymbol{W}''(s'')} \tag{D 1}$$

in which γ is the unit vector normal to the plane of the triad, whereas $\boldsymbol{\beta}$, $\boldsymbol{\beta}'$, $\boldsymbol{\beta}''$ are unit vectors normal to respectively $\boldsymbol{k}$, $\boldsymbol{p}$, $\boldsymbol{q}$ in the plane of the triad. Accordingly,

scalar products in terms of $\boldsymbol{k}$, $\boldsymbol{p}$, $\boldsymbol{q}$, $\boldsymbol{W}$, $\boldsymbol{W}'$, $\boldsymbol{W}''$, only depend on the moduli k, p and q. Starting from

$$g_{s's''} = -\tfrac{1}{4} P_{jlm}(\boldsymbol{k}) N_j(\boldsymbol{k}) N_n(-\boldsymbol{k}) N_l(s'\boldsymbol{p}) N_k(-s'\boldsymbol{p}) P_{rkn}(\boldsymbol{q}) N_m(s''\boldsymbol{q}) N_r(-s''\boldsymbol{q})$$

one finds that terms like $\mathrm{e}^{\mathrm{i}\lambda}$ are multiplied by their conjugate, so that only the $\boldsymbol{W}$ vectors remain. Therefore $g_{s's''}$ may be expressed in terms of the k, p and q only as

$$g_{s's''}(k,p,q) = \frac{1}{(4kpq)^2}[(p+q)^2-k^2][k^2-(p-q)^2][s'p-k][s'p-s''q][k+s'p+s''q]^2 \tag{D 2}$$

Not surprisingly, this geometric factor coincides with the one involved in EDQNM$_{2-3}$ when Z and h are ignored, which is $g_{s's''} = -C_{kpq}^2 A_1(k, s''q, s'p)/4$ with $C_{kpq} = \sin(\widehat{\boldsymbol{p},\boldsymbol{q}})/k = \sin(\widehat{\boldsymbol{k},\boldsymbol{q}})/p = \sin(\widehat{\boldsymbol{k},\boldsymbol{p}})/q$ and $A_1(k,p,q) = -(p-q)(k-q)(k+p+q)^2$, according to equations (A3) to (A5) in the appendix of Cambon *et al.* (1997), using $(p+q)^2 - k^2 = 2pq[1+\cos(\widehat{\boldsymbol{p},\boldsymbol{q}})]$ and $k^2-(p-q)^2 = 2pq[1-\cos(\widehat{\boldsymbol{p},\boldsymbol{q}})]$.

Appendix E. Numerics and validation

E.1. *Numerical method*

In equation (4.1), the time derivative is estimated with a first-order forward time scheme $(\partial_t e)(t) \simeq (e(t)+\Delta t) - e(t))/\Delta t$. The viscous term is centred in time and computed as $\nu k^2(e(t)+e(t+\Delta t))$. The energy transfer term is estimated explicitly, i.e. at time t from the known spectrum $e(t)$.

As mentioned in § 4, the spatial discretization uses wavevectors normalized by the base-wavenumber k, since all the triads with a given base-wavenumber polar angle θ are homologous. The discrete wavenumbers are $K_j = (k_{\min}/k)\exp(j\varepsilon_\rho)$ with $j \in \{0,\ldots,M_\rho\}$, and the logarithmic step is computed from the limit wavenumbers: $\varepsilon_\rho = \log(k_{\max}/k_{\min})/M_\rho$. The polar direction is discretized with $\theta_p = (p-1/2)\varepsilon_\theta$ where $p \in \{1,\ldots,M_\theta\}$ and $\varepsilon_\theta = \pi/M_\theta$, and we use the same discretization for the azimuthal angles ϕ_n with $n \in \{1,\ldots,M_\phi\}$. These two angles theoretically evolve between 0 and π, but numerically the smallest discretized angles are $\varepsilon_\phi/2$ and $\varepsilon_\theta/2$, and the largest ones $\pi-\varepsilon_\phi/2$ and $\pi-\varepsilon_\theta/2$.

Once the discretization is chosen with M_ρ, M_θ and M_ϕ, the numerical procedure starts with selecting which grid boxes intersect the resonant surface, by computing the characteristic function $F_{s's''}$ on the edges of the elementary volume. A change of sign indicates that the resonant surface cuts through the elementary box, and one computes the corresponding surface contribution by assuming the resonant surface to be plane within the box. The projected area of this plane onto one side of the box is first computed, and multiplied by the cosine of the projection angle to give the actual elementary surface contribution.

In the dynamical equation (4.1), the base wavevectors $\boldsymbol{k}$ scan the discretized space defined above, and within a given $e(\boldsymbol{k})$ equation, the discretized $\boldsymbol{p}$ in the energy transfer lie on the grid points. Thus the corresponding spectral energies $e(\boldsymbol{k})$ and $e(\boldsymbol{p})$ are well-defined. This is not the case for $e(\boldsymbol{q})$ which has to be interpolated over the available discretized values, by a second-order interpolation scheme.

Every time $\boldsymbol{q}$ falls out of the discretized space, representing triadic interactions with very small or very large wavenumbers, i.e. mainly non-local interactions, the corresponding energy is neglected.

E.2. *Validation procedure*

Before producing the definite results with a fixed set of computational parameters presented in this paper, we have thoroughly investigated the dependence of our numerical scheme on changes in the parameters. We have successively adopted two points of view.

First, using the initial analytical spectrum proposed by Orszag (1969), with unit peak wavenumber and energy (see the first spectrum of figure 4*a*), which yields the energy-density spectrum $e(\boldsymbol{k})$, we have compared the various transfer spectra $T(\boldsymbol{k})$ (right-hand side of equation (4.1)) obtained with different values of the numerical discretization parameters M_ρ, M_θ and M_ϕ. Starting with a given arbitrary choice $M_\rho = M_\theta = M_\phi = 100$, each of the parameters is gradually increased independently in turn, until a comparison of the values of the two transfer spectra at coincident points shows no significant change. (The difference is computed as $||T - T_{\mathrm{ref}}||/||T_{\mathrm{ref}}||$ with a suitable norm.) One then chooses the new value of the discretization parameter as the reference, and a fresh batch of computations of $T(\boldsymbol{k})$ is undertaken with this reference set of parameters. This not only provides a means of evaluating the dependence of the method's accuracy on each parameter, but also permits choice of optimal values in view of the computational cost. The influence of $k_{\min}$ and $k_{\max}$ is assessed in the same way.

Three such series of tests have allowed us to move from the initial values to $M_\rho = 200$, $M_\theta = M_\phi = 100$, then to $M_\rho = 400$, $M_\theta = 300$ and $M_\phi = 200$, and finally to $M_\rho = 400$, $M_\theta = 600$ and $M_\phi = 200$. The initial values 0.01 and 100 for the minimal and maximal wavenumbers have been changed to 0.1 and 10 in the procedure. (All the figures, and an extensive presentation of the method, are available in Bellet 2003.)

At the same time, the integral of each energy transfer over wave space is computed to check how well energy conservation is satisfied for each run. The convergence with increasing M_ρ is plotted on figure 1.

The second point of view for the study of the numerical scheme concerns the time dependent spectrum. The effective Reynolds number is first chosen to be $Re = 1$, with the same discretization parameters as above, and $\Delta t = 0.01$, and the computation goes to the final time $t_f = 0.38$. The influence of the time step is studied by decreasing the initial value, and appears to be small, so this value is kept. Then, again, the influence of the spatial resolution is studied in a series of non-stationary computations, with M_ρ increased up to 800, and M_θ to 900. (The influence of M_ϕ was shown in the previous runs to be negligible once the chosen value 100 was reached.) In these runs, the round-off errors and the radial cutoff at large wavenumbers are identified to be possible sources of numerical problems in the large wavenumber range of the spectrum, showing the necessity of a well-chosen $k_{\max}$. (We have tested values of up to $k_{\max} = 60$.)

For this reason, in view of the available computational resources, and in order to be able to continue the final computation as long as possible in time, we have only slightly increased the value of the effective Reynolds number to $Re = 5$ to take advantage of the stabilizing role of viscosity at very small scale. The reference case whose results are presented in this work also uses $M_\rho = 400$, $M_\theta = 300$, $M_\phi = 100$, $k_{\min} = 0.1$, $k_{\max} = 60$ and $\Delta t = 5 \times 10^{-5}$. The run is performed from the initial time $t = 0$ to $t_f = 1.05$.

REFERENCES

Babin, A., Mahalov, A. & Nicolaenko, B. 1997 Regularity and integrability of three-dimensional Euler and Navier-Stokes equations for uniformly rotating fluids. *Asympt. Anal.* **15** (2), 103–150.

Babin, A., Mahalov, A. & Nicolaenko, B. 1999 Global regularity of three-dimensional rotating Navier-Stokes equations for resonant domains. *Indiana Univ. Maths J.* **48** (3), 1133–1176.

Babin, A., Mahalov, A. & Nicolaenko, B. 2001 3D Navier-Stokes and Euler equations with initial data characterized by uniformly large vorticity. *Indiana Univ. Maths J.* **50**, 1–35.

Bardina, J., Ferziger, J. & Rogallo, R. S. 1985 Effect of rotation on isotropic turbulence: computation and modelling. *J. Fluid Mech.* **154**, 321–326.

Bartello, P., Métais, O. & Lesieur, M. 1994 Coherent structures in rotating three-dimensional turbulence. *J. Fluid Mech.* **173**, 1–29.

Bellet, F. 2003 Étude asymptotique de la turbulence d'ondes en rotation. PhD thesis, École Centrale de Lyon.

Benney, D. J. & Newell, A. C. 1969 Random wave closures. *Stud. Appl. Maths* **48**, 29–53.

Benney, D. J. & Saffman, P. G. 1966 Nonlinear interaction of random waves in a dispersive medium. *Proc. R. Soc. Lond.* A **289**, 301–320.

Caillol, P. & Zeitlin, V. 2000 Kinetic equations and stationary energy spectra of weakly nonlinear internal gravity waves. *Dyn. Atmos. Oceans* **32**, 81–112.

Cambon, C. 1982 Étude spectrale d'un champ turbulent incompressible soumis à des effets couplés de déformation et de rotation imposés extérieurement. PhD thesis, Univ. Lyon I, France.

Cambon, C., Godeferd, F. S., Nicolleau, F. C. G. A. & Vassilicos, J. C. 2004*a* Turbulent diffusion in rapidly rotating flows with and without stable stratification. *J. Fluid Mech.* **499**, 231–255.

Cambon, C. & Jacquin, L. 1989 Spectral approach to non-isotropic turbulence subjected to rotation. *J. Fluid Mech* **202**, 295–317.

Cambon, C., Jacquin, L. & Lubrano, J.-L. 1992 Toward a new reynolds stress model for rotating turbulence. *Phys. Fluids* A **4** (4), 812–824.

Cambon, C., Mansour, N. N. & Godeferd, F. S. 1997 Energy transfer in rotating turbulence. *J. Fluid Mech.* **337**, 303–332.

Cambon, C., Rubinstein, R. & Godeferd, F. S. 2004*b* Advances in wave turbulence: rapidly rotating flows. *New J. Phys.* **6** (73).

Cambon, C. & Scott, J. F. 1999 Linear and nonlinear models of anisotropic turbulence. *Annu. Rev. Fluid Mech.* **31**, 1–53.

Comte-Bellot, G. & Corrsin, S. 1971 Simple eulerian time-correlation of full and narrow-band velocity signals in grid-generated isotropic turbulence. *J. Fluid Mech.* **48**, 273–337.

Craya, A. D. D. 1958 Contribution à l'analyse de la turbulence associée à des vitesses moyennes. PST 345. Ministère de l'air, France.

Galtier, S. 2003 A weak inertial wave turbulence theory. *Phys. Rev.* E **68**, 015301-1–4.

Galtier, S., Nazarenko, S., Newell, A. C. & Pouquet, A. 2000 A weak turbulence theory for incompressible MHD. *J. Plasma Phys.* **63**, 447–488.

Godeferd, F. S. & Cambon, C. 1994 Detailed investigation of energy transfers in homogeneous stratified turbulence. *Phys. Fluids* **6** (6), 2084–2100.

Godeferd, F. S. & Staquet, C. 2003 Statistical modelling and direct numerical simulations of decaying stably-stratified turbulence. Part 2. Large-scale and small-scale anisotropy. *J. Fluid Mech.* **486**, 115–159.

Godeferd, F. S. & Lollini, L. 1999 Direct numerical simulations of turbulence with confinement and rotation. *J. Fluid Mech.* **393**, 257–308.

Greenspan, H. P. 1968 *The Theory of Rotating Fluids*. Cambridge University Press; reprinted 1990 by Breukelen Press, Brookline, MA.

Hossain, M. 1994 Reduction in the dimensionality of turbulence due to a strong rotation. *Phys. Fluids* **6**, 1077–1080.

Jacquin, L., Leuchter, O., Cambon, C. & Mathieu, J. 1990 Homogeneous turbulence in the presence of rotation. *J. Fluid Mech.* **220**, 1–52.

Kraichnan, R. H. 1958 The structure of isotropic turbulence at very high reynolds numbers. *J. Fluid Mech.* **5**, 497–543.

Leith, C. E. 1971 Atmospheric predicability and two dimensional turbulence. *J. Atmos. Sci.* **28**, 145–161.

Lvov, Y. & Tabak, E. 2001 Hamiltonian formalism and the garrett-munk spectrum of internal waves in the ocean. *Phys. Rev. Lett.* **87**, 168501.

McEwan, A. D. 1970 Inertial oscillations in a rotating fluid cylinder. *J. Fluid Mech.* **40**, 603–640.

Monin, A. & Yaglom, A. 1975 *Statistical Fluid Mechanics: Mechanics of Turbulence* (2 vols.). MIT Press.

Morinishi, Y., Nakabayashi, K. & Ren, S. Q. 2001*a* Dynamics of anisotropy on decaying homogeneous turbulence subjected to system rotation. *Phys. Fluids* **13**, 2912.

Morinishi, Y., Nakabayashi, K. & Ren, S. Q. 2001*b* A new dns algorithm for rotating homogeneous turbulence. *Intl J. Heat Fluid Flow* **22**, 30–38.

Mowbray, D. E. & Rarity, D. E. 1967 A theoretical and experimental investigation of the phase configuration of internal waves of small amplitude in a density stratified liquid. *J. Fluid Mech.* **28**, 1–16.

Orszag, S. A. 1969 Numerical methods for the simulation of turbulence. *Phys. Fluids, Suppl. II* **12**, 250–257.

Orszag, S. A. 1970 Analytical theories of turbulence. *J. Fluid Mech.* **41**, 363.

Pouquet, A., Lesieur, M., André, J. C. & Basdevant, C. 1975 Evolution of high Reynolds number two-dimensional turbulence. *J. Fluid Mech.* **75**, 305–319.

Reynolds, W. C. & Kassinos, S. 1995 One-point modeling for rapidly deformed homogeneous turbulence. *Proc. R. Soc. Lond.* A **451**, 87–104.

Riley, J. J., Metcalfe, R. W. & Weissman, M. A. 1981 Direct numerical simulations of homogeneous turbulence in density-stratified fluids. In *Proc AIP Conf. on Nonlinear Properties of Internal Waves* (ed. B. West), pp. 79–112. American Institute of Physics.

Smith, L. & Lee, Y. 2005 On near resonances and symmetry breaking in forced rotating flows at moderate rossby number. *J. Fluid Mech.* **535**, 111–142.

Smith, L. & Waleffe, F. 1999 Transfer of energy to two-dimensional large scales in forced, rotating three-dimensionnal turbulence. *Phys. Fluids* **11** (6), 1608–1622.

Smith, L. & Waleffe, F. 2002 Generation of slow large scales in forced rotating stratified turbulence. *J. Fluid Mech.* **451**, 145–168.

Squires, K. D., Chasnov, J. R., Mansour, N. N. & Cambon, C. 1994 The asymptotic state of rotating homogeneous turbulence at high Reynolds number. In *Application of Direct and Large Eddy Simulation to Transition and Turbulence*. Chania, Crete, Greece.

Staquet, C. & Sommeria, J. 2002 Internal gravity waves: from instabilities to turbulence. *Annu. Rev. Fluid Mech.* **34**, 559–593.

Turner, L. 1999 Macroscopic structures of inhomogeneous, Navier-Stokes turbulence. *Phys. Fluids* **11**, 2367–2380.

Waleffe, F. 1993 Inertial transfers in the helical decomposition. *Phys. Fluids* A **5**, 677–685.

Yang, X. & Domaradzki, J. A. 2004 LES of decaying rotating turbulence. *Phys. Fluids* **16**, 4088–4104.

Zakharov, V. E., Lvov, V. & Falkovich, G. 1992 *Wave turbulence*. Springer.

Zhou, Y. 1995 A phenomenological treatment of rotating turbulence. *Phys. Fluids* **7**, 2092.